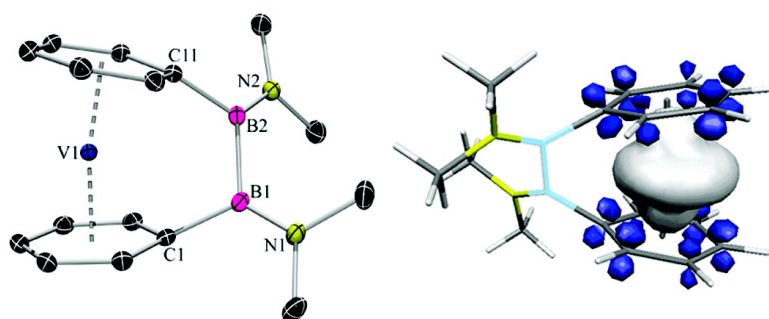**Article**

Synthesis, Reactivity, and Electronic Structure of [*n*]Vanadoarenophanes: An Experimental and Theoretical Study

Holger Braunschweig, Martin Kaupp, Christopher J. Adams,
Thomas Kupfer, Krzysztof Radacki, Sandra Schinzel, and

More About This Article

Additional resources and features associated with this article are available within the HTML version:

- Supporting Information
- Links to the 2 articles that cite this article, as of the time of this article download
- Access to high resolution figures
- Links to articles and content related to this article
- Copyright permission to reproduce figures and/or text from this article

View the Full Text HTML

Synthesis, Reactivity, and Electronic Structure of [*n*]Vanadoarenophanes: An Experimental and Theoretical Study

Holger Braunschweig,*,[†] Martin Kaupp,*,[†] Christopher J. Adams,[‡] Thomas Kupfer,[†] Krzysztof Radacki,[†] and Sandra Schinzel[†]

Institut für Anorganische Chemie, Julius-Maximilians-Universität Würzburg, Am Hubland, D-97074 Würzburg, Germany, and School of Chemistry, University of Bristol, Cantock's Close, Bristol, BS8 1TS, U.K.

Received March 19, 2008; E-mail: h.braunschweig@mail.uni-wuerzburg.de; kaupp@mail.uni-wuerzburg.de

Abstract: An optimized procedure for the selective dimetalation of $[V(\eta^6\text{-}C_6H_6)_2]$ by BuLi/tmeda allowed for the isolation and characterization of $[V(\eta^6\text{-}C_6H_5Li)_2]\cdot$tmeda. X-ray diffraction of its thf solvate $[V(\eta^6\text{-}C_6H_5Li)_2]\cdot(thf)_7$ revealed an unsymmetrical, dimeric composition in the solid state, in which both subunits are connected by three bridging lithium atoms. Treatment with several element dihalides facilitated the isolation of [*n*]vanadoarenophanes (*n* = 1, 2) with boron and silicon in the bridging positions. In agreement with the number and covalent radii of the bridging elements, these derivatives exhibit molecular ring strain to a greater or lesser extent. The B–B bond of the [2]bora species $[V(\eta^6\text{-}C_6H_5)_2B_2(NMe_2)_2]$ was readily cleaved by $[Pt(PEt_3)_3]$ to afford the corresponding oxidative addition product. Subsequently, $[V(\eta^6\text{-}C_6H_5)_2B_2(NMe_2)_2]$ was employed as a diborane(4) precursor in the diboration of 2-butyne under stoichiometric, homogeneous, and heterogeneous catalysis conditions. This transformation is facilitated by the reduction of molecular ring strain, which was confirmed by a decrease of the tilt angle α observed in the corresponding solid-state structures. EPR spectroscopy was used to probe the electronic structure of strained [*n*]vanadoarenophanes and revealed an obvious correlation between the degree of molecular distortion and the observed hyperfine coupling constant a_{iso}. State-of-the-art DFT calculations were able to reproduce the measured isotropic vanadium hyperfine couplings and the coupling anisotropies. The calculations confirmed the decrease of the absolute isotropic hyperfine couplings with increasing tilt angle. Closer analysis showed that this is mainly due to increased positive contributions to the spin density at the vanadium nucleus from the spin polarization of doubly occupied valence orbitals of vanadium-ligand σ-antibonding character. The latter are destabilized and thus made more polarizable in the bent structures.

Introduction

The discovery of ferrocene, $[Fe(\eta^5\text{-}C_5H_5)_2]$, by Kealy and Pauson in 1951[1] and the publication of bis(benzene)chromium, $[Cr(\eta^6\text{-}C_6H_6)_2]$, four years later by Fischer and Hafner[2] initiated studies of a new class of organometallic complexes containing cyclic π-coordinated ligands. The initial findings prompted huge research efforts in this area and resulted in the preparation of numerous ring-substituted derivatives including ansa-bridged type systems, which have recently been of growing interest owing to their unique structure, bonding, and reactivity patterns.[3] In particular, the development of the ring-opening polymerization (ROP) of strained [1]silaferrocenophanes in 1992[4] highlighted strained [*n*]metalloarenophanes as efficient precursors for metal-containing macromolecules.[5,6] It has also been impressively demonstrated over the past decade that the molecular ring strain present in [*n*]metalloarenophanes is accompanied by

Scheme 1. Selective Dimetalation of Ferrocene Employing BuLi/tmeda
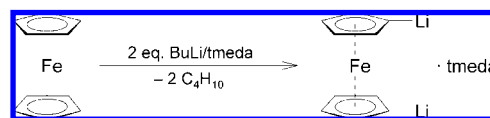
enhanced reactivity of either the bonds between the carbocyclic ligands and the bridging element(s),[7] of those between the bridging elements,[8] or of those between the metal center and one of the carbocyclic ligands,[9] facilitating a very interesting insertion and substitution chemistry. In general, the preparation of ansa complexes is accomplished by stoichiometric salt-elimination reactions of dimetalated sandwich complexes with element dihalides and hence requires the availability of selectively 1,1′-dimetalated and well-defined metallocene precursors. In this context, the first report of the selective dilithiation of ferrocene was an early and important achievement (Scheme 1).[10] Subsequently, the double deprotonation of several other homoleptic and heteroleptic sandwich complexes became accessible by employing alkyl lithium bases in the presence of a coordinating amine such as *N,N,N′,N′*-tetramethylethylenediamine (tmeda) or *N,N,N′,N″,N″*-pentamethyldiethylenetriamine (pmdta). How-

---

[†] Julius-Maximilians-Universität Würzburg.
[‡] University of Bristol.
(1) Kealy, T. J.; Pauson, P. L. *Nature* **1951**, *168*, 1039.
(2) (a) Fischer, E. O.; Hafner, Z. Z. *Naturforsch.* **1955**, *10b*, 665. (b) Fischer, E. O.; Hafner, Z. Z. *Anorg. Allg. Chem.* **1956**, *286*, 146. (c) Seyferth, D. *Organometallics* **2002**, *21*, 1520. (d) Seyferth, D. *Organometallics* **2002**, *21*, 2800.

ever, because of their high reactivity, the structural elucidation of these species is still the subject of considerable inquiry. With the exception of $[Fe(\eta^5\text{-}C_5H_4Li)_2]\cdot(pmdta)$[11] and $[Fe(\eta^5\text{-}C_5H_4Li)_2]_3\cdot(tmeda)_2$,[12] reports on the successful isolation and structural characterization appeared only recently in the literature. For instance, we were able to determine the solid-state structures of dilithiated $[Cr(\eta^6\text{-}C_6H_6)_2]$,[8f] $[Mo(\eta^6\text{-}C_6H_6)_2]$,[13]

$[Cr(\eta^5\text{-}C_5H_5)(\eta^7\text{-}C_7H_7)]$,[14] and $[Mn(\eta^5\text{-}C_5H_5)(\eta^6\text{-}C_6H_6)_2]$.[15] Important contributions also came from Mulvey and co-workers with the selective mono-, di-, and tetrametalation of ferrocene as well as the synergic monodeprotonation of $[Cr(\eta^6\text{-}C_6H_6)_2]$, which were accomplished under more complex reaction conditions.[16] Selective dimetalation of ferrocene was also achieved by alkali−metal-mediated manganation, in which case manganese was for the first time directly attached to an aromatic framework.[17] In addition, transmetalation reactions of tin-substituted ferrocene derivatives and pentafluorophenylcopper, $[C_6F_5Cu]_4$, to yield selectively mono- and dimetalated ferrocenyl−copper complexes were described lately by Jäkle et al.[18] A related compound was obtained by Wagner and co-workers by transmetalation of $[Fe(\eta^5\text{-}C_5H_4Li)_2]_3\cdot(tmeda)_2$ with $FeCl_2$ to afford a pentanuclear Fe^{II} cluster with two bridging iron centers.[19]
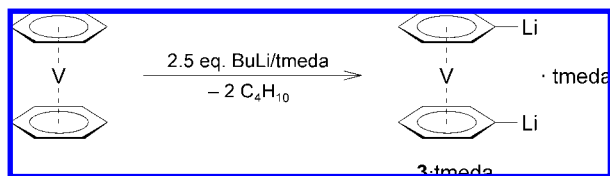
In the course of our recent studies on strained [*n*]metalloarenophanes, we became interested in paramagnetic ansa complexes, particularly those derived from bis(benzene)vanadium, $[V(\eta^6\text{-}C_6H_6)_2]$. This vanadium-$d^5$ system bears one unpaired electron and has already been employed in the synthesis of several [1]vanadoarenophanes containing Al,[20] Ga,[20] Si,[21] Ge,[22] and Zr[23] in bridging positions, although its reactivity has not been investigated in detail. Structural data available to date are in agreement with the anticipated strained character that is reflected by tilt angles α ranging from 3.7 to 20.2° in the zirconium- and silicon-bridged compounds, respectively. EPR spectroscopic studies carried out primarily by Elschenbroich and co-workers provided insight into the electronic structure of these derivatives and revealed an obvious correlation of the electronic parameters with the degree of molecular distortion,[21a,23] as well as highly interesting intermetallic communication in some dinuclear species.[21b,c]
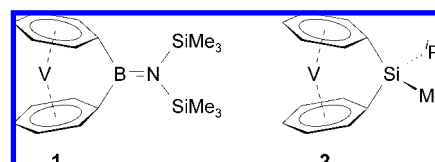
Very recently, we reported on the synthesis and characterization of the highly strained [1]bora- and [1]silavanadoarenophanes

(3) (a) Osborne, A. G.; Whiteley, R. H. *J. Organomet. Chem.* **1975**, *101*, C27. (b) Seyferth, D.; Whiters, H. P. *Organometallics* **1982**, *1*, 1275. (c) Elschenbroich, C.; Hurley, J.; Metz, B.; Massa, W.; Baum, G. *Organometallics* **1990**, *9*, 889. (d) Buretea, M. A.; Tilley, T. D. *Organometallics* **1997**, *16*, 1507. (e) Hultzsch, K. C.; Nelson, J. M.; Lough, A. J.; Manners, I. *Organometallics* **1995**, *14*, 5496. (f) Rulkens, R.; Gates, D. P.; Balaishis, D.; Pudelski, J. K.; McIntosh, D. F.; Lough, A. J.; Manners, I. *J. Am. Chem. Soc.* **1997**, *119*, 10976. (g) Jäkle, F.; Rulkens, R.; Zech, G.; Foucher, D. A.; Lough, A. J.; Manners, I. *Chem.−Eur. J.* **1998**, *4*, 2117. (h) Braunschweig, H.; Breitling, F. M.; Gullo, E.; Kraft, M. *J. Organomet. Chem.* **2003**, *680*, 31. (i) Aldridge, S.; Bresner, C. *Coord. Chem. Rev.* **2003**, *244*, 71. (j) Braunschweig, H.; Homberger, M.; Hu, C.; Zheng, X.; Gullo, E.; Clentsmith, G. K. B.; Lutz, M. *Organometallics* **2004**, *23*, 1968. (k) Schachner, J. A.; Lund, C. L.; Quail, J. W.; Müller, J. *Organometallics* **2005**, *24*, 785. (l) Herbert, D. E.; Mayer, U. F. J.; Manners, I. *Angew. Chem.* **2007**, *119*, 5152; *Angew. Chem., Int. Ed.* **2007**, *46*, 5060.

(4) (a) Foucher, D. A.; Tang, B.-Z.; Manners, I. *J. Am. Chem. Soc.* **1992**, *114*, 6246.

(5) (a) Nguyen, P.; Gómez-Elipe, P.; Manners, I. *Chem. Rev.* **1999**, *99*, 1515. (b) Manners, I. *Chem. Commun.* **1999**, 857. (c) MacLachlan, M. J.; Ginzburg, M.; Coombs, N.; Coyle, T. W.; Raju, N. P.; Greedan, J. E.; Ozin, G. A.; Manners, I. *Science* **2000**, *287*, 1460. (d) Manners, I. *Science* **2001**, *294*, 1664. (e) Arsenault, A. C.; Mı́guez, H.; Kitaev, V.; Ozin, G. A.; Manners, I. *Adv. Mater.* **2003**, *15*, 503. (f) Clendenning, S. B.; Han, S.; Coombs, N.; Paquet, C.; Rayat, M. S.; Grozea, D.; Brodersen, P. M.; Sodhi, R. N. S.; Yip, C. M.; Lu, Z.-H.; Manners, I. *Adv. Mater.* **2004**, *16*, 291. (g) Bellas, V.; Rehahn, M. *Angew. Chem.* **2007**, *119*, 5174; *Angew. Chem., Int. Ed.* **2007**, *46*, 5082.

(6) It should be noted that the borylene-bridged poly(ferrocenylene)s were obtained by a different approach via polycondensation reactions. Heilmann, J. B.; Scheibnitz, M.; Qin, Y.; Sundararaman, A.; Jäkle, F.; Kretz, T.; Bolte, M.; Lerner, H.-W.; Holthausen, M. C.; Wagner, M. *Angew. Chem.* **2006**, *118*, 934; *Angew. Chem., Int. Ed.* **2006**, *46*, 920.

(7) (a) Sheridan, J. B.; Lough, A. J.; Manners, I. *Organometallics* **1996**, *15*, 2195. (b) Mizuta, T.; Yamasaki, T.; Nakazawa, H.; Miyoshi, K. *Organometallics* **1996**, *15*, 1093. (c) Sheridan, J. B.; Temple, K.; Lough, A. J.; Manners, I. *J. Chem. Soc., Dalton Trans.* **1997**, 711. (d) Jäkle, F.; Rulkens, R.; Zech, G.; Foucher, D. A.; Lough, A. J.; Manners, I. *Chem.−Eur. J.* **1998**, *4*, 2117. (e) Mizuta, T.; Onishi, M.; Miyoshi, K. *Organometallics* **2000**, *19*, 5005. (f) Mizuta, T.; Onishi, M.; Nakazono, T.; Nakazawa, H.; Miyoshi, K. *Organometallics* **2002**, *21*, 717. (g) Tamm, M.; Kunst, A.; Herdtweck, E. *Chem. Commun.* **2005**, 1729.

(8) (a) Finckh, W.; Tang, B. Z.; Lough, A. J.; Manners, I. *Organometallics* **1992**, *11*, 2904. (b) Herberhold, M.; Steffl, U.; Milius, W.; Wrackmeyer, B. *Angew. Chem.* **1997**, *109*, 1545; *Angew. Chem., Int. Ed.* **1997**, *36*, 1508. (c) Braunschweig, H.; Lutz, M.; Radacki, K. *Angew. Chem.* **2005**, *117*, 5792; *Angew. Chem., Int. Ed.* **2005**, *44*, 5647. (d) Braunschweig, H.; Lutz, M.; Radacki, K.; Schaumlöffel, A.; Seeler, F.; Unkelbach, C. *Organometallics* **2006**, *25*, 4433. (e) Braunschweig, H.; Kupfer, T.; Lutz, M.; Radacki, K.; Seeler, F.; Sigritz, R. *Angew. Chem.* **2006**, *118*, 8217; *Angew. Chem., Int. Ed.* **2006**, *45*, 8048. (f) Braunschweig, H.; Kupfer, T. *Organometallics* **2007**, *26*, 4634.

(9) (a) Braunschweig, H.; Dirk, R.; Englert, U.; Berenbaum, A.; Green, J. C.; Lough, A. J.; Manners, I. *J. Am. Chem. Soc.* **2000**, *122*, 5765. (b) Mizuta, T.; Imamura, Y.; Miyoshi, K. *J. Am. Chem. Soc.* **2003**, *125*, 2068. (c) Tanabe, M.; Bourke, S. C.; Herbert, D. E.; Lough, A. J.; Manners, I. *Angew. Chem.* **2005**, *117*, 6036; *Angew. Chem., Int. Ed.* **2005**, *44*, 5886.

(10) Rausch, M. D.; Ciappenelli, D. J. *J. Organomet. Chem.* **1967**, *13*, 127.

(11) Walczak, M.; Walczak, K.; Mink, R.; Rausch, M. D.; Stucky, G. *J. Am. Chem. Soc.* **1978**, *100*, 6382.

(12) Butler, I. R.; Cullen, W. R.; Ni, J.; Rettig, S. J. *Organometallics* **1985**, *4*, 2196.

(13) Braunschweig, H.; Buggisch, N.; Englert, U.; Homberger, M.; Kupfer, T.; Leusser, D.; Lutz, M.; Radacki, K. *J. Am. Chem. Soc.* **2007**, *129*, 4840.

(14) Braunschweig, H.; Kupfer, T.; Lutz, M.; Radacki, K. *J. Am. Chem. Soc.* **2007**, *129*, 8893.

(15) Braunschweig, H.; Kupfer, T.; Radacki, K. *Angew. Chem.* **2007**, *119*, 1655; *Angew. Chem., Int. Ed.* **2007**, *46*, 1630.

(16) (a) Clegg, W.; Henderson, K. W.; Kennedy, A. R.; Mulvey, R. E.; O'Hara, C. T.; Rowlings, R. B.; Tooke, D. M. *Angew. Chem.* **2001**, *113*, 4020; *Angew. Chem., Int. Ed.* **2001**, *40*, 3902. (b) Henderson, K. W.; Kennedy, A. R.; Mulvey, R. E.; O'Hara, C. T.; Rowlings, R. B. *Chem. Commun.* **2001**, 1678. (c) Andrikopoulos, P. C.; Armstrong, D. R.; Clegg, W.; Gilfillan, C. J.; Hevia, E.; Kennedy, A. R.; Mulvey, R. E.; O'Hara, C. T.; Parkinson, J. A. *J. Am. Chem. Soc.* **2004**, *126*, 11612. (d) Hevia, E.; Honeyman, G. W.; Kennedy, A. R.; Mulvey, R. E.; Sherrington, D. C. *Angew. Chem.* **2005**, *117*, 70; *Angew. Chem., Int. Ed.* **2005**, *44*, 68. (e) Garcia-Álvarez, J.; Kennedy, A. K.; Klett, J.; Mulvey, R. E. *Angew. Chem.* **2007**, *119*, 1123; *Angew. Chem., Int. Ed.* **2007**, *46*, 1105.

(17) Garcia-Álvarez, J.; Kennedy, A. K.; Klett, J.; Mulvey, R. E. *Angew. Chem.* **2007**, *119*, 1123; *Angew. Chem., Int. Ed.* **2007**, *46*, 1105.

(18) Venkatasubbaiah, K.; DiPasquale, A. G.; Bolte, M.; Rheingold, A. L.; Jäkle, F. *Angew. Chem.* **2006**, *118*, 6992; *Angew. Chem., Int. Ed.* **2006**, *45*, 6838.

(19) Sänger, I.; Heilmann, J. B.; Bolte, M.; Lerner, H.-W.; Wagner, M. *Chem. Commun.* **2006**, 2027.

(20) Lund, C. L.; Schachner, J. A.; Quail, J. W.; Müller, J. *Organometallics* **2006**, *25*, 5817.

Scheme 2. Selective Dimetalation of [V(η^6-C$_6$H$_6$)$_2$]

Figure 1. Molecular structure of [V(η^6-C$_6$H$_5$Li)$_2$]$_2$·(thf)$_7$ (3·thf) in the solid state. Only the oxygen atoms of the thf molecules are shown. For clarity, hydrogen atoms and thf molecules incorporated in the crystal lattice are omitted. Selected bond lengths (Å) and angles (deg): Li1−Li2 3.0987(69), Li1−Li4 2.4031(68), Li3−Li4 2.5107(80), Li1−C20 2.1061(54), Li1−C30 2.2599(53), Li1−C40 2.1406(52), Li2−C40 2.1563(57), Li3−C10 2.1635(56), Li3−C30 2.4450(63), Li4−C10 2.1986(59), Li4−C20 2.2362(58), Li4−C30 2.2551(55), V2−X$_{Ph1}$ 1.668, V2−X$_{Ph2}$ 1.667, V1−X$_{Ph3}$ 1.672, V1−X$_{Ph4}$ 1.667, C20−Li1−C30 111.11(23), C20−Li1−C40 148.65(27), C30−Li1−C40 98.54(21), C10−Li3−C30 100.70(22), C10−Li4−C20 96.95(21),C10−Li4−C30 105.82(25),C20−Li4−C30 106.62(22),C10−Li4−O70 122.42(25), C20−Li4−O70 111.32(27), C30−Li4−O70 111.91(24), X$_{Ph1}$−V2−X$_{Ph2}$ 177.8, X$_{Ph3}$−V1−X$_{Ph4}$ 179.1 (X$_{Ph1}$ = centroid of the C$_6$H$_5$ ring C10−C15, X$_{Ph2}$ = centroid of the C$_6$H$_5$ ring C20−C25, X$_{Ph3}$ = centroid of the C$_6$H$_5$ ring C30−C35, X$_{Ph4}$ = centroid of the C$_6$H$_5$ ring C40−C45).

1 and **2**, and their reactivity toward low-valent transition-metal complexes.[24] Whereas reaction of **2** with Karstedt's catalyst allowed for the preparation of a soluble organometallic polymer containing paramagnetic repeat units via ROP, **1** underwent a stoichiometric ring-opening reaction under similar conditions. In this contribution, we report full details of our work on the synthesis and structural characterization of some [1]- and [2]vanadoarenophanes, as well as on the isolation and solid-state structure of the dimetalated bis(benzene)vanadium precursor. In addition, we demonstrate the suitability of [2]boravanadoarenophane to act as a diborane(4) precursor in the diboration of alkynes under both homogeneous and heterogeneous catalysis conditions. We also present detailed studies of the electronic structure of these molecules, which was investigated by means of EPR spectroscopy and DFT calculations.

Results and Discussion

Dimetalation of [V(η^6-C$_6$H$_6$)$_2$]. Since the first report on the selective dimetalation of [V(η^6-C$_6$H$_6$)$_2$] by Elschenbroich and Gerson in 1974,[25] the resulting reaction product has occasionally been employed in the preparation of ring-substituted derivatives including several ansa complexes.[20–23] However, the material thus obtained was usually neither isolated nor characterized, but reacted in situ with various element (di)halides. From the nature of the isolated products, the formation of a dilithiated metallocene intermediate appears to be substantiated, although the exact composition has never been investigated. In our hands, a facile and selective double deprotonation of [V(η^6-C$_6$H$_6$)$_2$] was achieved by treatment of the sandwich complex with 2.5 equiv of BuLi and tmeda in heptane at elevated temperatures (80 °C) over a period of 16 h to afford the base-stabilized complex [V(η^6-C$_6$H$_5$Li)$_2$]·tmeda (3·tmeda). Compound 3·tmeda is thermally stable under an inert atmosphere and can be isolated as a brown, pyrophoric powder in high yields up to 90% (Scheme 2).

The formulation as [V(η^6-C$_6$H$_5$Li)$_2$]·tmeda (i.e., the coordination of one molecule tmeda per [V(η^6-C$_6$H$_5$Li)$_2$] moiety) is supported by both elemental analysis and trapping reactions with H$_2$O. The selectivity of the dimetalation is further confirmed by the molecular structure of **3** in the solid state (Figure 1). Recrystallization of 3·tmeda from a saturated thf solution at −80 °C afforded dark red crystals that were suitable for X-ray

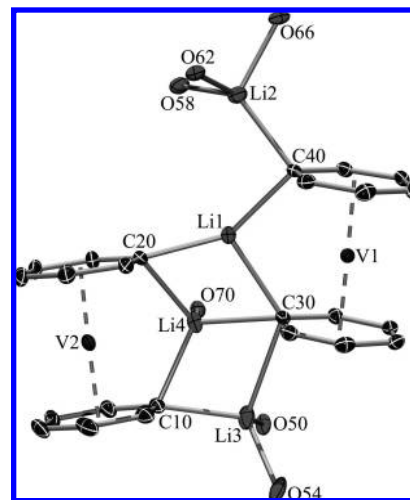diffraction. **3** crystallizes isostructural to the corresponding chromium derivative[8f] in the triclinic space group $P\bar{1}$ as its thf adduct [V(η^6-C$_6$H$_5$Li)$_2$]·(thf)$_7$ (3·thf) (i.e., dissolving in thf causes the replacement of the tmeda ligand by coordinating thf molecules). The solid-state structure consists of two bis(benzene)vanadium fragments deprotonated in the 1,1′ positions, which are linked by two bridging (Li1 and Li4), one semibridging (Li3), and one terminal lithium atom (Li2). The unsaturated Li centers are stabilized by the coordination to the anionic C$_{ipso}$ atoms of the C$_6$H$_5$ moieties and to the thf oxygen atoms. The coordinated thf molecules show extensive disorder, thus requiring a combination of constraints and restraints in the refinement, and as a consequence, their structural parameters are excluded from the following discussion.

As expected, the structural parameters of the bis(benzene)-vanadium fragments are in agreement with the unstrained character of a 1,1′-disubstituted sandwich complex. Accordingly, the V−CH bond lengths are found within a narrow range between 2.1716(32) and 2.1989(27) Å, while the V−C$_{ipso}$ distances are significantly longer [between 2.2355(25) and 2.2482(25) Å], a fact that is attributable to the anionic character of the deprotonated carbon atoms. Moreover, the carbocyclic ligands of each [V(η^6-C$_6$H$_5$)$_2$] moiety are arranged almost parallel with angles between the planes of the C$_6$H$_5$ rings of 0.7 and 2.2°, respectively. The angles δ, defined by the ring centroids and the metal center, indicate almost linear arrangements (δ = 179.1 and 177.8°). In accordance with the molecular structure of [Cr(η^6-C$_6$H$_5$Li)$_2$]·(thf)$_7$,[8f] four different lithium environments can be distinguished: (i) Both bis(benzene)vanadium subunits act as bidentate ligands to one of the bridging Li atoms through the deprotonated ipso carbons (Li1, C30 and C40; Li4, C10 and C20) and further stabilize the other bridging

(21) (a) Elschenbroich, C.; Hurley, J.; Metz, B.; Massa, W.; Baum, G. *Organometallics* **1990**, *9*, 889. (b) Elschenbroich, C.; Bretschneider-Hurley, A.; Hurley, J.; Massa, W.; Wocadlo, S.; Pebler, J. *Inorg. Chem.* **1993**, *32*, 5421. (c) Elschenbroich, C.; Bretschneider-Hurley, A.; Hurley, J.; Behrendt, A.; Massa, W.; Wocadlo, S.; Reijerse, E. *Inorg. Chem.* **1995**, *34*, 743.
(22) Elschenbroich, C.; Schmidt, E.; Gondrum, R.; Metz, B.; Burghaus, O.; Massa, W.; Wocadlo, S. *Organometallics* **1997**, *16*, 4589.
(23) Elschenbroich, C.; Schmidt, E.; Metz, B.; Harms, H. *Organometallics* **1995**, *14*, 4043.
(24) Braunschweig, H.; Adams, C. J.; Kupfer, T.; Manners, I.; Richardson, R.; Whittell, G. R. *Angew. Chem.* **2008**, *120*, 3886; *Angew. Chem., Int. Ed.* **2008**, *47*, 3826.
(25) Elschenbroich, C.; Gerson, F. *Chimia* **1974**, *28*, 720.

Scheme 3. Syntheses of [n]Vanadoarenophanes (n = 1,2)

Scheme 4. Decomposition of [n]Vanadoarenophanes **4**−**6** upon Air Exposure
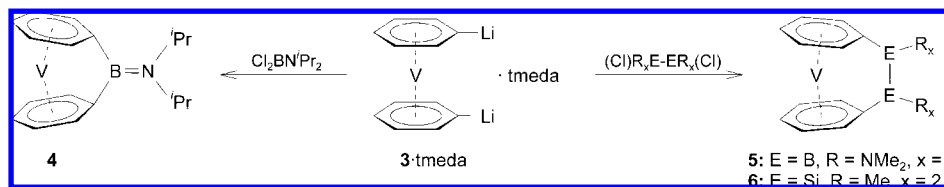
lithium atom by coordination of the inner C_{ipso} atoms (Li1−C20; Li4−C30). The unsaturated bridging lithium atom Li1 remains three-coordinate and is found in a distorted trigonal planar environment (Σ = 358.2°). (ii) By contrast, Li4 is four-coordinate and exhibits, as expected, a distorted tetrahedral geometry with one additional thf molecule on the fourth coordination site. (iii) The terminal lithium center Li2 is bound to the ipso carbon of one six-membered ring and is further stabilized by the coordination of three thf oxygen atoms, thus being in a tetrahedral environment. (iv) The semibridging lithium atom adopts a highly distorted tetrahedral geometry. Coordination both to the oxygen atoms of two thf molecules and to the C_{ipso} atoms of two different C_6H_5 rings is found to be necessary for stabilization. The Li⋯C bond distance Li3⋯C30 [2.4450(62) Å] is notably elongated with respect to the other Li−C bonds (vide infra), but significantly shorter than the related Li2⋯C20 contact [4.250 Å]. Similar stabilization effects were observed in the solid-state structure of $[Fe(\eta^5-C_5H_4Li)_2]_3\cdot(tmeda)_2$.[12] According to the authors, the interaction serves to complete the tetrahedral coordination sphere of the unsaturated lithium center via η^1-bonding to the anionic carbon atom or by an agostic Li⋯C−H interaction. Hence, both the relatively short Li1⋯C30 separation distance and the absence of hydrogen atoms bound to C30 suggest that this stabilizing interaction also exists in **3**·thf and consists most probably of a η^1-bonding mode to the deprotonated carbon atom C30. The other Li−C bond lengths [2.1061(54)−2.2599(53) Å],[8f,11–15] as well as the Li−O bond distances [1.9582(69)−2.0070(59) Å][26] lie within previously reported ranges. In agreement with the structural parameters of related dilithiated sandwich complexes, the Li⋯Li separation distances of the bridging and semibridging lithium centers Li1, Li2, and Li4 [Li1⋯Li4, 2.4031(68) Å; Li3⋯Li4, 2.5107(80) Å] differ significantly from that of the terminal lithium atom [Li1⋯Li2, 3.0987(69) Å] and thus might suggest a stabilizing lithium−lithium interaction. However, as pointed out earlier, this type of stabilization is expected to be weak at best.[27]

[n]Vanadoarenophanes (n = 1, 2). With this well-defined species in hand, the synthesis of ansa-bridged derivatives is straightforward, and we recently communicated the facile conversion of **3**·tmeda to the corresponding [1]vanadoarenophanes with boron (**1**) and silicon (**2**) in the bridging position.[24] Accordingly, stoichiometric reactions of **3**·tmeda with the appropriate element dihalides at −78 °C in aliphatic solvents such as heptane afforded the [1]bora- (**4**), [2]bora- (**5**), and [2]silavanadoarenophanes (**6**) as highly colored, deep-red to black crystalline materials in moderate to good yields, respectively (Scheme 3).
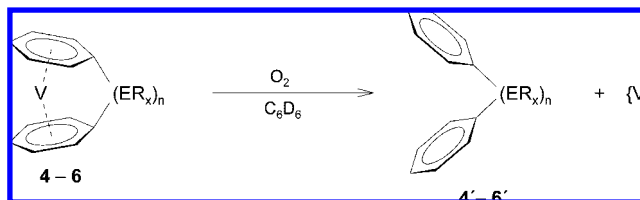
Compounds **4**−**6** were unambiguously identified by elemental analysis, mass spectrometry, and EPR spectroscopy (vide infra). These species turned out to be thermally very robust, which, for instance, enabled the observation of the molecular ions M^+ [m/z = 316 (**4**), 315 (**5**), 321 (**6**)] with high intensities in the corresponding mass spectra, as well as coherent fragmentation patterns. Since the characteristic resonances for the η^6-coordinated ligands cannot be observed in the NMR spectra of **4**−**6**, presumably because of paramagnetic line broadening, NMR samples were also prepared under air exposure, which resulted in the instantaneous decomposition of the ansa complexes accompanied by the appearance of a black precipitate and a colorless solution. According to NMR spectroscopy, the supernatant consisted of the free ligands $Ph_2BN^iPr_2$, (NMe₂)PhB-BPh(NMe₂), and PhMe₂Si-SiMe₂Ph (**4′**−**6′**; Scheme 4), whereas the exact nature of the vanadium-containing precipitate has not been clarified to date. The relative integration ratios of the observed signals are in agreement with the presence of two phenyl groups in each case that are not coordinated to a transition-metal center (**4′**: δ = 7.06−7.24 ppm; **5′**: δ = 7.29−7.39 ppm; **6′**: δ = 7.21−7.36 ppm; each m, 10H). Hence, controlled decomposition of paramagnetic [n]vanadoarenophanes represents another valuable characterization technique that might be useful in cases where X-ray diffraction data are not available.

To authenticate the formation of ansa-bridged complexes, the molecular structures of **4**−**6** were determined in the solid state by X-ray diffraction. **4** crystallizes in the monoclinic space group $P2_1/n$ with two independent molecules in the asymmetric unit, with the structural parameters of the two moieties only marginally different. Hence, for simplicity reasons, only one of the molecular structures is discussed below (Figure 2). The incorporation of the small boron ansa bridge results in a substantial deviation of the aromatic rings from the coplanar arrangement observed in the parent sandwich complex. The most prominent structural feature is given by the tilting of the two carbocyclic ligands and, hence, by the presence of molecular ring strain, which is represented by the tilt angle α = 29.44(6)°. As expected, this value is comparable to that found in the previously described complex $[V(\eta^6-C_6H_5)_2BN(SiMe_3)_2]$ (**1**; α = 31.12°),[24] just like all other structural parameters. Because of the smaller covalent radius of the boron nucleus and the greater interannular distance in bis(benzene)vanadium, both the related [1]silavanadoarenophanes (α = 19−20°)[21] and the corresponding [1]borachromoarenophanes (α = 26.6°)[3i] are significantly less tilted.

(26) (a) Hoppe, I.; Marsch, M.; Harms, K.; Boche, G.; Hoppe, D. *Angew. Chem.* **1995**, *107*, 2328; *Angew. Chem., Int. Ed.* **1995**, *34*, 2158. (b) Wiberg, N.; Hwang-Park, H.-S.; Mikulcik, P.; Müller, G. *J. Organomet. Chem.* **1996**, *511*, 239. (c) Nanjo, M.; Nanjo, E.; Mochida, K. *Eur. J. Inorg. Chem.* **2004**, 2961.

(27) (a) Brown, T. L.; Seitz, L. M.; Kimura, B. Y. *J. Am. Chem. Soc.* **1968**, *90*, 3245. (b) Scovell, B. Y.; Kimura, B. Y.; Spiro, T. G. *J. Coord. Chem.* **1971**, *1*, 107.
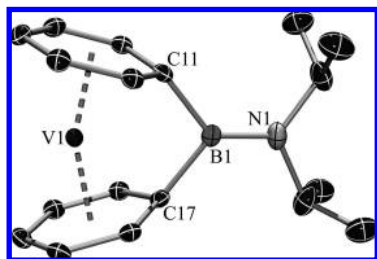
Figure 2. Molecular structure of $[V(\eta^6\text{-}C_6H_5)_2BN^iPr_2]$ (**4**) in the solid state. For clarity, only one of the molecules in the asymmetric unit is shown and hydrogen atoms are omitted. Selected bond lengths (Å) and angles (deg): V1−C11 2.1408(18), V1−C12 2.1677(18), V1−C13 2.2150(18), V1−C14 2.2442(18), V1−C15 2.2373(19), V1−C16 2.1797(18), V1−C17 2.1336(17), V1−C18 2.1708(18), V1−C19 2.2320(18), V1−C20 2.2437(18), V1−C21 2.2343(18), V1−C22 2.1721(18), C11−B1 1.6057(27), C17−B1 1.6040(27), B1−N1 1.3779(26), V1−X_{Ph1} 1.674, V1−X_{Ph2} 1.674, C11−B1−C17 101.46(14), C11−B1−N1 131.60(18), C17−B1−N1 126.81(17), X_{Ph1}−V1−X_{Ph2} 156.9, α = 29.44(6) (X_{Ph1} = centroid of the C_6H_5 ring C11−C16, X_{Ph2} = centroid of the C_6H_5 ring C17−C22).

Bis(benzene)vanadium (332 pm) and ferrocene (335 pm), however, feature similar interannular distances, and therefore, the molecular distortion of **4** is similar to that of the corresponding [1]boraferrocenophane (α = 32.4°).[9a] Directly associated with the tilted structure of **4**, the angle δ is reduced to 156.9° in comparison to those observed in the unstrained derivative $[V(\eta^6\text{-}C_6H_5)_2ZrCp'_2]$ (Cp′ = C_5H_4-^{t}Bu; δ = 176.3°)[23] and bis(benzene)vanadium (δ = 180°).[28] The highly strained character is also illustrated by the very short V−C_{ipso} bond lengths [2.1408(18) and 2.1336(17) Å] with respect to the V−C_{para} bond distances [2.2442(18) and 2.2437(18) Å], although the average V−C distance (2.197 Å) remains unaffected compared to the unstrained species mentioned above. However, the carbocyclic π-ligands are virtually planar and can be considered as primarily η^6-coordinated. The geometry around the bridging boron atom also emphasizes the high degree of molecular distortion. Even though the B−N bond length [1.3982(27) Å] as well as the trigonal-planar environment of the boron center (Σ = 360°) are in agreement with the formulation of a B=N double bond, the C_{Ph}−B−C_{Ph} angle θ of 101.46(14)° is conspicuously diminished from the ideal angle of 120° expected for an sp^2-hybridized boron atom. Concomitantly, the C_{Ph}−B−N bond angles are widened to values of 126.81(17)° and 131.60(18)°.

The solid-state structure of **5** reveals a less distorted geometry in comparison to that of **4**, which is already implicated by the larger dimension of the diborane ansa bridge (Figure 3). However, the π-coordinated C_6H_5 moieties show a significant degree of tilting with respect to each other by an angle of α = 14.40(5)°. As expected, this value is substantially smaller than that observed in the [1]bora derivative **4** [α = 29.44(6)°], indicating the presence of less molecular strain. The corresponding chromium congener $[Cr(\eta^6\text{-}C_6H_5)_2B_2(NMe_2)_2]$[3i] exhibits significantly less structural distortion and consequently a diminished tilt angle α = 10.1° with respect to **5**, which is again related to the increased interannular distance of $[V(\eta^6\text{-}C_6H_6)_2]$ (332 pm) compared to that of bis(benzene)chromium (322 pm). Surprisingly, even though ferrocene features a greater interannular distance (335 pm), the tilting of the aromatic ligands in **5** is more pronounced than that in the corresponding [2]boraferrocenophane, which is manifested by a smaller value of the tilt
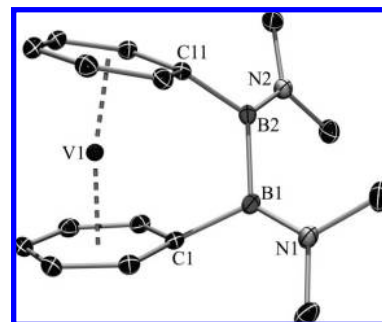

Figure 3. Molecular structure of $[V(\eta^6\text{-}C_6H_5)_2B_2(NMe_2)_2]$ (**5**) in the solid state. Hydrogen atoms are omitted for clarity. Selected bond lengths (Å) and angles (deg): V1−C1 2.1715(10), V1−C2 2.1629(10), V1−C3 2.2205(11), V1−C4 2.2287(11), V1−C5 2.2194(10), V1−C6 2.1992(11), V1−C11 2.1758(9), V1−C12 2.2042(10), V1−C13 2.2214(10), V1−C14 2.2297(10), V1−C15 2.2185(11), V1−C16 2.1635(10), C1−B1 1.5870(16), C11−B2 1.5863(15), B1−B2 1.7175(17), B1−N1 1.4033(15), B2−N2 1.4045(15), V1−X_{Ph1} 1.676, V1−X_{Ph2} 1.678, C1−B1−B2 108.58(9), C11−B2−B1 107.96(8), X_{Ph1}−V1−X_{Ph2} 169.5, C1−B1−B2−C11 50.12(11), X_{Ph1}−C1−C11−X_{Ph2} 23.4, α = 14.40(5) (X_{Ph1} = centroid of the C_6H_5 ring C1−C6, X_{Ph2} = centroid of the C_6H_5 ring C11−C16).

angle α = 12.8° in the latter.[29] This fact can readily be explained by the high flexibility of the diatomic B−B bridge. As indicated by the torsion angle C1−B1−B2−C11, this flexibility results in a significant twisting of the ansa bridge by 50.12(11)°. By contrast, this value is essentially reduced to −42.27° in the ferrocene derivative, and hence the smaller tilt angle in comparison to **5** appears plausible. The moderate ring strain is also reflected by the angle δ = 169.5°, which is larger than that in the [1]boravanadoarenophane **4**, but still differs noticeably from the linear arrangement of the parent sandwich complex. Likewise, the geometry around the bridging boron centers deviates far less from the ideal sp^2-hybridization with respect to the molecular structure of **4**. The boron atoms show trigonal-planar environments (B1, Σ = 359°; B2, Σ = 359°), and the respective bond angles [between 107.96(8)° and 128.48(10)°] are found to be much closer to the expected value of 120°.

As expected given the greater covalent radius of silicon, the solid-state structure of the Si−Si-bridged [2]vanadoarenophane **6** reveals only a minor distortion of the molecular geometry with respect to $[V(\eta^6\text{-}C_6H_6)_2]$. Accordingly, the angle between the planes of the carbocyclic ligands is just 4.38(11)°, and **6** should not be considered as a strained ansa complex. The values reported for the analogous [2]ferrocenophane (α = 4.19°)[30] and [2]trovacenophane (α = 3.80°)[31] lie within a similar range, and those for the corresponding [2]chromoarenophanes (α = 2.60 and 2.78°)[8f,32] and [2]nickelocenophane (α = 9.37°)[30] are slightly smaller or notably larger, respectively. The unstrained character is also supported by the angle δ = 176.8°, which is substantially widened compared to that of the [1]- and [2]bo-

(28) Fischer, E. O.; Fritz, H. P.; Manchot, J.; Priebe, E.; Schneider, R. *Chem. Ber.* **1963**, *96*, 1418.

(29) Braunschweig, H.; Seeler, F.; Sigritz, R. *J. Organomet. Chem.* **2007**, *692*, 2354.

(30) (a) Dement'ev, V. V.; Cervantes-Lee, F.; Parkanyi, L.; Sharma, H.; Pannell, K. H. *Organometallics* **1993**, *12*, 1983. (b) Finckh, W.; Tang, B.-Z.; Foucher, D. A.; Zamble, D. B.; Ziembinski, R.; Lough, A. J.; Manners, I. *Organometallics* **1993**, *12*, 823.
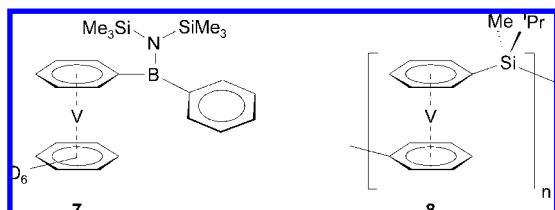
(31) Elschenbroich, C.; Paganelli, F.; Nowotny, M.; Neumüller, B.; Burghaus, O. *Z. Anorg. Allg. Chem.* **2004**, *630*, 1599.

(32) Bartole-Scott, A.; Braunschweig, H.; Kupfer, T.; Lutz, M.; Manners, I.; Nguyen, T.-I.; Radacki, K.; Seeler, F. *Chem.−Eur. J.* **2006**, *12*, 1266.

(33) Braunschweig, H.; Gross, M.; Radacki, K. *Organometallics* **2007**, *26*, 6688.

ravanadoarenophanes **4** and **5**, and which almost reaches the linear alignment of the parent sandwich complex. In addition, the V−C$_{ipso}$ [2.1995(21) and 2.1979(22) Å] and V−C$_{para}$ [2.2091(23) and 2.2117(23) Å] bonds feature nearly equal distances, which markedly contrasts with the results discussed above. The absence of ring strain is further reflected by the geometry around the silicon atoms that display an approximately ideal tetrahedral environment, where the largest discrepancy is found for the C$_{ipso}$−Si−Si angles [C11−Si1−Si2, 103.81(7)°; C21−Si2−Si1, 103.36(7)°]. The two benzene rings adopt an eclipsed position, highlighted by the torsion angle C11−Si1−Si2−C21 equal to 0.00°, which is in contrast to the twisted conformation described for the [2]bora derivative **5** [50.12(11)°]. A similar observation was reported earlier for the corresponding chromium complexes.[8f]

Reactivity. Recently, we described our studies on the reactivity of [1]bora- (**1**) and [1]silavanadoarenophanes (**2**) toward low-valent platinum complexes.[24] Whereas treatment of **1** with catalytic amounts of [Pt(PEt$_3$)$_3$] afforded the ring-opened product **7**, reaction of **2** with Karstedt's catalyst at slightly elevated temperatures yielded the soluble paramagnetic polymer **8** (M_n > 28 000 g mol^{-1}). Hence, current work has focused on the reactivity of the [2]boravanadoarenophane **5** under similar conditions. In particular, the suitability of **5** to act as a diborane(4) precursor in the functionalization of alkynes was of interest, since related diboron-bridged ansa complexes have proven to be susceptible to strain release by undergoing transition-metal-catalyzed diboration reactions under both homogeneous and heterogeneous catalysis conditions.[8e] Employing **5** as a diborane(4) precursor would offer the possibility of preparing bis(boryl)alkenes containing a paramagnetic transition-metal backbone.

To substantiate whether the B−B bond of **5** can be activated for further functionalization reactions, **5** was reacted with stoichiometric amounts of [Pt(PEt$_3$)$_3$] at 85 °C in benzene over a period of 48 h, which resulted in the oxidative addition of the B−B bond to the Pt(0) center. Recrystallization from heptane afforded the [3]platinadibora derivative **9** as a deep-red crystalline material in high yields of 87% (Scheme 5).

According to mass spectrometry, **9** proved to be thermally much more labile than the [n]vanadoarenophanes **1**−**7**, and only decomposition products could be observed in its mass spectrum. However, the identity was unambiguously confirmed by means of elemental analysis, EPR spectroscopy (vide infra), and crystal structure analysis (Figure 5). The driving force of this transformation is given both by the reduction of molecular ring strain and by the formation of two stable Pt−B bonds. Thus, the insertion of the [Pt(PEt$_3$)$_2$] fragment into the strained B−B bond is accompanied by a reduction of the tilt angle α = 6.15(44)°, as well as by a widening of the deformation angle δ = 175.2° with respect to **5** [α = 14.40(5)°; δ = 169.5°]. Similar values have been observed for complexes that participate in analogous reactions of the Fe and Cr congeners.[8e] In agreement with the unstrained character of **9**, the π-coordinated ligands are arranged

Scheme 5. Oxidative Cleavage of the B−B Bond and Formation of *ansa*-Bis(boryl)alkene **10**
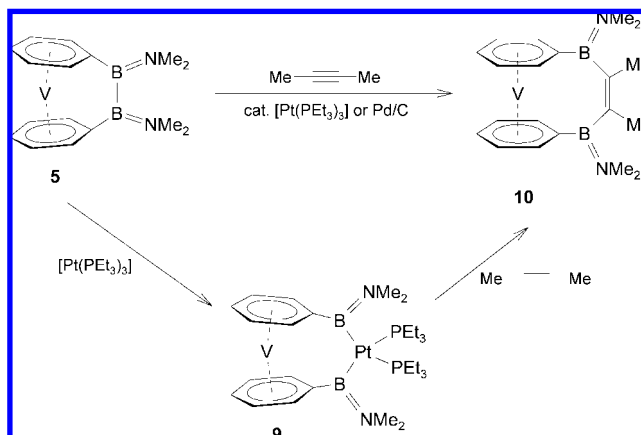
Figure 4. Molecular structure of [V(η^6-C$_6$H$_5$)$_2$Si$_2$Me$_4$] (**6**) in the solid state. Symmetry-related positions (x, $-y$ + 3/2, z) are labeled with _a. Hydrogen atoms are omitted for clarity. Selected bond lengths (Å) and angles (deg): V1−C11 2.1995(21), V1−C12 2.1961(15), V1−C13 2.2088(15), V1−C14 2.2091(23), V1−C21 2.1979(22), V1−C22 2.1902(15), V1−C23 2.2033(15), V1−C24 2.2117(23), C11−Si1 1.8852(22), C21−Si2 1.8924(23), Si1−Si2 2.3422(8), V1−X$_{Ph1}$ 1.681, V1−X$_{Ph2}$ 1.676, C11−Si1−Si2 103.81(7), C21−Si2−Si1 103.36(7), X$_{Ph1}$−V1−X$_{Ph2}$ 176.8, C11−Si1−Si2−C21 0.00, X$_{Ph1}$−C11−C21−X$_{Ph2}$ 0.00, α = 4.38(11) (X$_{Ph1}$ = centroid of the C$_6$H$_5$ ring C11−C14, X$_{Ph2}$ = centroid of the C$_6$H$_5$ ring C21−C24).

almost parallel to each other, and consequently, the V−C bond distances are found within a narrow interval [2.1775(70)−2.2030(75) Å]. The boron centers feature a trigonal-planar geometry (B1, Σ = 360°; B2, Σ = 360°), which indicates an almost regular sp^2-hybridization of the boron atoms. The Pt center displays a distorted square-planar environment, and the Pt−B [Pt1−B1, 2.1241(86) Å; Pt1−B2, 2.1225(69) Å] and Pt−P bond distances [Pt1−P1, 2.3441(15) Å; Pt1−P2, 2.3310(18) Å], as well as the B1−Pt1−B2 [76.76(30)°] and P1−Pt1−P2 bond angles [97.67(7)°] lie within the expected ranges.[8e,34]

Reaction of **9** with a 10-fold excess of 2-butyne in benzene at 75 °C for 24 h resulted in the formation of the *ansa*-bis(boryl)alkene **10** and the reductive elimination of the [Pt-(PEt$_3$)$_2$] fragment. Compound **10** was isolated analytically pure after recrystallization from hexanes as black crystals in 63% yield (Scheme 5). Attempts to obtain higher yields were thwarted by the similar solubilities of **10** and the platinum-containing

(34) (a) Irvine, G. J.; Lesley, M. J. G.; Marder, T. B.; Norman, N. C.; Rice, C. R.; Robins, E. G.; Roper, W. R.; Whittell, G. R.; Wright, L. J. *Chem. Rev.* **1998**, *98*, 2685. (b) Lu, N.; Norman, N. C.; Orpen, A. G.; Quayle, M. J.; Timms, P. L.; Whittell, G. R. *J. Chem. Soc., Dalton Trans.* **2000**, 4032. (c) Curtis, D.; Lesley, M. J. G.; Norman, N. C.; Orpen, A. G.; Starbuck, J. *J. Chem. Soc., Dalton Trans.* **1999**, 1687. (d) Iverson, C. N.; Smith, M. R. *J. Am. Chem. Soc.* **1995**, *117*, 4403. (e) Lesley, G.; Nguyen, P.; Taylor, N. J.; Marder, T. B.; Scott, A. J.; Clegg, W.; Norman, N. C. *Organometallics* **1996**, *15*, 5137.
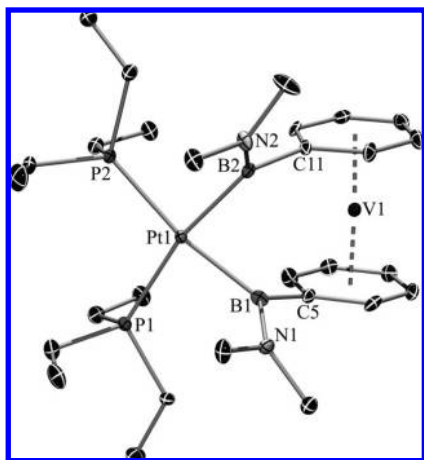
Figure 5. Molecular structure of [V(η^6-C$_6$H$_5$BNMe$_2$)Pt(PEt$_3$)$_2$(η^6-C$_6$H$_5$BNMe$_2$)] (**9**) in the solid state. Hydrogen atoms are omitted for clarity. Selected bond lengths (Å) and angles (deg): V1−C5 2.1925(72), V1−C6 2.1756(76), V1−C7 2.1891(78), V1−C8 2.2011(78), V1−C9 2.1936(68), V1−C10 2.1784(66), V1−C11 2.1929(73), V1−C12 2.1775(70), V1−C13 2.1895(68), V1−C14 2.2030(75), V1−C15 2.1990(75), V1−C16 2.1826(70), C5−B1 1.570(13), C11−B2 1.608(10), B1−N1 1.428(11), B2−N2 1.409(10), Pt1−B1 2.1241(86), Pt1−B2 2.1225(69), Pt1−P1 2.3441(15), Pt1−P2 2.3310(18), V1−X$_{Ph1}$ 1.661, V1−X$_{Ph2}$ 1.665, C5−B1−Pt1 117.70(51), C11−B2−Pt1 121.62(51), B1−Pt1−B2 76.76(30), P1−Pt1−P2 97.67(7), X$_{Ph1}$−V1−X$_{Ph2}$ 175.2, X$_{Ph1}$−C5−C11−X$_{Ph2}$ −8.6, α = 6.15(44) (X$_{Ph1}$ = centroid of the C$_6$H$_5$ ring C5−C10, X$_{Ph2}$ = centroid of the C$_6$H$_5$ ring C11−C16).

Figure 6. Molecular structure of [V(η^6-C$_6$H$_5$BNMe$_2$)C(Me)=C(Me)(η^6-C$_6$H$_5$BNMe$_2$)] (**10**) in the solid state. Hydrogen atoms are omitted for clarity. Selected bond lengths (Å) and angles (deg): V1−C11 2.2063(23), V1−C12 2.1879(22), V1−C13 2.1912(23), V1−C14 2.2067(23), V1−C15 2.2008(23), V1−C16 2.1791(24), V1−C21 2.1976(22), V1−C22 2.1729(25), V1−C23 2.1903(26), V1−C24 2.2098(23), V1−C25 2.2021(23), V1−C26 2.1764(22), C11−B1 1.5722(31), C21−B2 1.5805(34), B1−N1 1.3934(32), B2−N2 1.4030(31), B1−C7 1.5874(34), B2−C8 1.5877(34), C7−C8 1.3445(34), V1−X$_{Ph1}$ 1.672, V1−X$_{Ph2}$ 1.666, C11−B1−C7 118.25(21), C21−B2−C8 119.81(19), B1−C7−C8 121.71(21), B2−C8−C7 122.01(20), C5−C7−C8 123.28(17), C6−C8−C7 122.70(21), X$_{Ph1}$−V1−X$_{Ph2}$ 177.7, B1−C7−C8−C6 179.20(20), B1−C7−C8−B2 −2.41(34), C5−C7−C8−B2 177.51(22), C5−C7−C8−C6 −0.82(29), X$_{Ph1}$−C11−C21−X$_{Ph2}$ −0.4, α = 3.40(13) (X$_{Ph1}$ = centroid of the C$_6$H$_5$ ring C11−C16, X$_{Ph2}$ = centroid of the C$_6$H$_5$ ring C21−C26).

side products, although related studies employing the corresponding ferrocene and bis(benzene)chromium derivatives confirmed the quantitative conversion to the bisborylated products.[8e] The mass spectrum of **10** is in agreement with the proposed constitution and suggests a high thermal stability. Consequently, the molecular ion M$^+$ (m/z = 369) could be observed with an intensity of 100%. The EPR spectrum is consistent with the presence of an unstrained complex and will be discussed in detail later. In addition, the insertion of the alkyne is confirmed by the determination of the molecular structure by X-ray diffraction (Figure 6). The methyl groups of the bis(boryl)alkene moiety are arranged cis to each other, which is illustrated by torsion angles B1−C7−C8−B2 = −2.41(3)°, C11−B1−C7−C8 = −73.39(28)°, and C21−B2−C8−C7 = 79.25(29)°. According to the torsion angles B1−C7−C8−B2 = −2.41(34)°, B1−C7−C8−C6 = 179.20(20)°, C5−C7−C8−B2 = 177.51(22)°, and C5−C7−C8−C6 = −0.82(29)°, the alkene unit itself nearly adopts an ideal planar geometry. In addition, the bond angles found are in a narrow range and hence confirm the expected sp^2-hybridization of the alkene carbon atoms C7 and C8. Other relevant structural parameters include the B−C bond distances [1.5722(31)−1.5877(34) Å] and the C=C bond length [1.3445(34) Å], which lie in the typical range for B−C single bonds and C−C double bonds, respectively. While the [3]platinadibora derivative **9** features at least a small degree of ring strain, the introduction of a B−C=C−B bridge results in an almost parallel arrangement of the carbocyclic ligands in **10**. Thus, the tilt angle α = 3.40(13)° is reduced to some extent with respect to the starting material, whereas the deformation angle δ = 177.7 is marginally wider. These parameters are comparable to those found in the [2]silavanadoarenophane **6** and the ring-opened product **7**,[24] and hence prove the unstrained character of **10** that is also manifested by the regular trigonal-
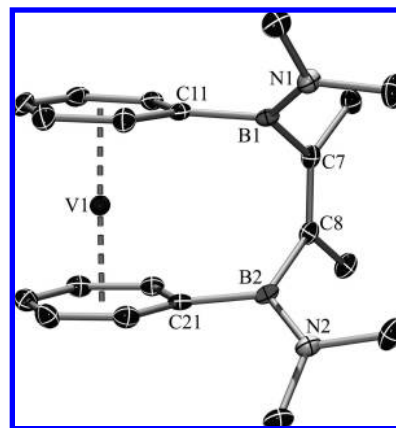
planar environment of the boron centers (B1, Σ = 360°; B2, Σ = 360°) and the adapted V−C bond lengths [2.1729(25)−2.2098(23) Å].

To confirm the anticipated propensity of the [2]boravanadoarenophane **5** to undergo transition-metal-mediated insertion of alkynes into the B−B bond under catalysis conditions, **5** was treated in subsequent experiments with 2-butyne in the presence of catalytic amounts of [Pt(PEt$_3$)$_3$] and Pd/C, respectively. The reaction conditions were chosen in analogy to those described for the chromium congener.[8e] For this purpose, a resealable NMR tube was charged with the ansa complex, a 10-fold excess of 2-butyne and 5 mol% [Pt(PEt$_3$)$_3$] or 6 mol% of Pd/C, and heated to 95 °C in benzene (Scheme 5). The conversions were found to be quantitative after 5 d for the homogeneous reaction ([Pt(PEt$_3$)$_3$]) and after 14 d for the heterogeneous reaction (Pd/C). The *ansa*-bis(boryl)alkene **10** was isolated analytically pure after workup in high yields of 90 and 93%, respectively. It should be noted that control experiments were carried out, which proved that **5** underwent no reaction with 2-butyne in the absence of a transition-metal catalyst.

UV−Vis Spectroscopy. To probe the electronic structure of the [n]vanadoarenophanes, solution UV−vis spectra in the range of 200−800 nm were collected in thf for the species **1**, **2**, **4−6**, **9**, and **10** (Table 1). Detailed UV−vis spectroscopic data of [V(η^6-C$_6$H$_6$)$_2$] were reported by Ozin and co-workers in 1986.[35] According to the authors, the absorption spectrum consists of three distinct regions: (i) A weak absorption at 445 nm, (ii) an intense band at 320 nm, and (iii) an intense, rising high-energy absorption commencing at 200 nm. The individual bands were assigned to the corresponding transitions in combination with MO calculations on the electronic structure of bis(benzene)vanadium. Hence, the lowest-energy absorption was assigned to

(35) Andrews, M. P.; Mattar, S. M.; Ozin, G. A. *J. Phys. Chem.* **1986**, *90*, 1037.

transitions arising from the singly occupied SOMO into MOs that are ligand in character, metal in character, as well as of mixed ligand−metal character. However, these transitions are either orbitally or Laporte forbidden, which is responsible for their weak intensities. The broad and intense transition occurring at 320 nm was attributed to a metal-to-ligand charge-transfer absorption and the remaining high-energy tail to additional charge-transfer and intraligand transitions. In particular, the weak, lowest-energy band represents a viable probe for the electronic structure of metallocenes and [n]metalloarenophanes, respectively, which is quite sensitive to changes in the structural parameters.[3e,14,36] For instance, it has been shown that bridging ferrocene by an ansa bridge results in a red-shift of the corresponding lowest-energy absorption and that this red-shift is correlated to the degree of molecular distortion (i.e., to the tilt angle α).[3e] However, we recently described the UV−vis spectra of a series of [n]trochrocenophanes and found that the substitution pattern of the ligands and the electronic environment of the bridging atom also exert strong influence on the absolute position of these absorbances.[14] Thus, the highly strained [1]bora (**1**, **4**) and [1]sila derivatives (**2**), which feature the most pronounced tilting of the carbocyclic ligands, exhibit visible bands at 416 and 428 nm, respectively, that are substantially blue-shifted in comparison to the absorbance observed for bis(benzene)vanadium. Surprisingly, the less strained [n]vanadoarenophanes **5**, **6**, **9**, and **10** ($n = 2−4$) show a complementary trend and the lowest-energy bands are actually red-shifted to 460, 467, 458, and 455 nm without any correlation to the tilt angle. Accordingly, the positions of these visible bands seem to depend on the number of bridging atoms, but appear to be independent of both the substitution pattern of the ligands and the exact value of the tilt angle. The reason for this behavior has not yet been clarified.

EPR Spectroscopy. As pointed out by Elschenbroich and co-workers, EPR spectroscopy is a valuable tool for the characterization of paramagnetic V(0)-d^5 sandwich complexes.[21–23,31] Analyses of the *g* tensor and the hyperfine coupling constant *a* have revealed detailed informations about the molecular structure and, particularly, the degree of tilting in ansa complexes derived from bis(benzene)vanadium and trovacene. In addition, EPR spectroscopic data provide information on the extent of metal−ligand spin delocalization and, thus, the electronic structure. Bridging an unsubstituted sandwich complex by an ansa bridge is accompanied by a transformation of the *g* tensor from axial ($g_{\parallel}$, $g_{\perp}$) to nonaxial (g_x, g_y, g_z) and in changes of the metal and ligand hyperfine coupling constants as a consequence of modified metal−ligand orbital overlap. Since the SOMO of bis(benzene)vanadium is primarily metal centered (d_{z^2}) and lies in the nodal plane of the ligand π-orbitals, the metal−ligand interaction is almost negligible. Bending of the carbocyclic ligands, however, results in the loss of axial symmetry and allows for the mixing of the metal and ligand orbitals. This has been thought to facilitate appreciable spin transfer from the singly occupied SOMO to the ligands, leading to a decrease of the metal hyperfine coupling constant. We will demonstrate below that enhanced spin polarization of doubly occupied valence orbitals in the bent complexes is even more important for the observed trends than spin delocalization of the SOMO. Previously reported EPR spectroscopic data of several [n]vanadoarenophanes are in agreement with these considerations.[21–23]

Table 1. Experimentally Determined UV−Vis Data

	1	2	4	5	6	9	10	BBV[a]
λ_{max} (nm)	416	428	416	460	467	458	455	445
ε (L mol^{-1}cm^{-1})	2265	2458	2753	2437	1671	2219	2130	1123
α (deg)	31.1	20.9[b]	29.4	14.4	4.4	6.2	3.4	0.0

[a] BBV = [V(η^6-C$_6$H$_6$)$_2$]. [b] Calculated value.

Thus, the hyperfine coupling constant a_{iso} in the [1]silavanadoarenophane [V(η^6-C$_6$H$_5$)$_2$SiPh$_2$] (**11**, α = 19.2°; a_{iso} = 56 G) is reduced with respect to the unstrained [V(η^6-C$_6$H$_6$)$_2$] (a_{iso} = 64 G).[21a] To further confirm this correlation, we determined the EPR spectra of **4**−**6**, **9**, and **10** in both fluid (240 K, toluene) and rigid solution (110−140 K, toluene). Relevant EPR parameters are summarized in Table 2. For the sake of completeness, the data of the previously reported derivatives **1**, **2**, **7**, and **8**, as well as those of [V(η^6-C$_6$H$_6$)$_2$] and **11** are also included for comparison.[37]

The isotropic EPR spectra recorded in fluid solution (toluene) at 240 K are fairly similar and feature well-resolved coupling to one ^{51}V-nucleus ($I = 7/2$) and asymmetric line broadening effects due to molecular rotation. Values for the *g* tensor are found in the same region (1.985−1.986) observed by Elschenbroich et al. for several other ansa-bridged bis(benzene)vanadium complexes.[21–23] The hyperfine coupling constants a_{iso}(^{51}V) reveal an excellent correlation with the corresponding tilt angles α (Figure 7); an increase of the tilting of the carbocyclic ligands is associated with a decrease of the observed hyperfine coupling constant. By contrast, none of the fluid EPR spectra exhibit additional proton hyperfine coupling to the hydrogen atoms of the π-coordinated ligands.

The anisotropic spectra were recorded in rigid solution (toluene) at 110−140 K and indicate, as expected, the presence of rhombic systems to a greater or lesser extent (i.e., the *x*, *y*, and *z* directions are different). The spectra are in agreement with the existence of a singly occupied d_{z^2} orbital, for which g_x, $g_y < g_z \approx 2.0023$ is anticipated. Because of the tilting of the aromatic rings, the degeneracy of the d_{xz} and d_{yz} orbitals is lifted, which allows for the differentiation of the *x* and *y* directions in both the *g* factors and the hyperfine coupling constant *a*. The splitting of *x* and *y* is noteworthy and has also been described by Elschenbroich et al. for the related germanium-bridged species[22] but was not detected for the silicon-bridged complex **11**.[21a] Even though one might expect a direct correlation between the extent of the splitting $\Delta a = a_x − a_y$ and the corresponding splitting of the *g* tensor $\Delta g = g_x − g_y$, as well as the tilt angle α, no evidence for that could be deduced from the EPR spectroscopic data. The observation of proton hyperfine coupling is limited to the anisotropic EPR spectrum of the previously reported [1]silavanadoarenophane **2**, which displays coupling to ten pseudoequivalent C$_6$H$_5$ protons [a(^{1}H) = 3.5 G].[24] Unresolved coupling of the same type probably accounts for the line width of the spectra for the boron-containing complexes.

DFT Calculations. DFT methods are applied here to investigate the origin of the correlation between the tilt angle α and vanadium hyperfine coupling by systematic analysis of the spin-density distribution and the associated ^{51}V hyperfine coupling tensors of compounds **1**, **2**, **4**−**7**, **10**, and [V(η^6-C$_6$H$_6$)$_2$]. Contributions from different orbitals are used to address the

(36) Tamm, M.; Kunst, A.; Bannenberg, T.; Herdtweck, E.; Sirsch, P.; Elsevier, C. J.; Ernsting, J. M. *Angew. Chem.* **2004**, *116*, 5646; *Angew. Chem., Int. Ed.* **2004**, *43*, 5530.

(37) Graphical representations of the EPR spectra of **2** in both fluid and rigid solutions are given in the Supporting Information as representative examples.

Table 2. EPR Parameters for **1**, **2**, **4**−**11**, and [V(η^6-C$_6$H$_6$)$_2$]

	1	2	4	5	6	7	8	9	10	11	BBV[d]
α (deg)	31.1	na[c]	29.4	14.4	4.4	5.6		6.2	3.4	19.2	0
g_{iso}	1.985	1.985	1.985	1.986	1.985	1.985		1.986	1.986	1.987	1.986
a_{iso} (G)[a]	54.5	56.9	53.75	59.6	61.5	63.7		64.0	63.0	56.3	63.8
g_x	1.975	1.975	1.973	1.976	1.976	1.976	1.987	1.976	1.978		
g_y	1.977	1.977	1.976	1.979	1.976	1.976		1.980	1.979	1.979[e]	1.978[e]
g_z	2.001	1.999	2.001	1.998	2.001	2.001		1.998	2.001	2.002[f]	2.001[f]
$\langle g \rangle$[b]	1.985	1.984	1.983	1.985	1.984	1.984		1.985	1.986		
a_x (G)[a]	87.5	89.0	89.3	89.0	91.0	95.8		93.5	95.5		
a_y (G)[a]	74.0	83.0	74.3	86.0	91.0	88.0		88.0	88.7	85.0[g]	92.5[g]
a_z (G)[a]	1.5	−3.0	1.5	1.0	1.0	1.5		0.5	1.0	0[h]	0.6[h]
$\langle a \rangle$[a,b]	54.3	56.3	55.0	58.7	61.0	61.8		60.7	61.7		
T (K)	140	110	110	130	110	110	110	140	110	130	130
lit.	24	24	i	i	i	24	24	i	i	i	21a

[a] a(^{51}V). [b] Mean value. [c] Not available. [d] BBV = [V(η^6-C$_6$H$_6$)$_2$]. [e] $g_\parallel$. [f] $g_\perp$. [g] $a_\parallel$. [h] $a_\perp$. [i] This work.
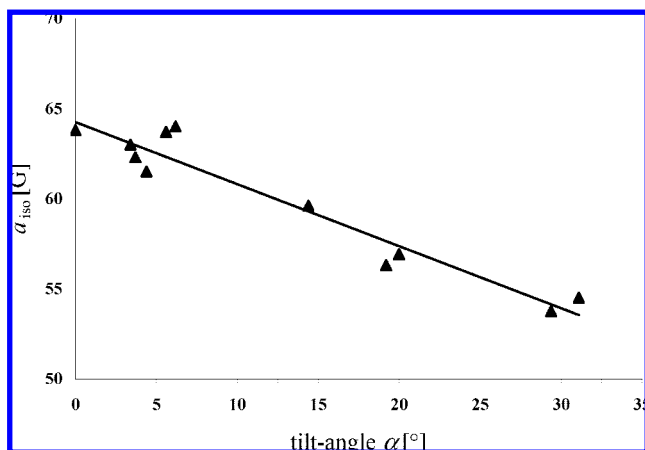
Figure 7. Hyperfine coupling constants a_{iso} (G) as a function of the tilt angle α (deg).

Table 3. Mulliken Atomic Spin Densities and $\langle S^2 \rangle$ Expectation Values for [V(η^6-C$_6$H$_5$)$_2$BN(SiMe$_3$)$_2$] (**1**)

	$\rho^{\alpha-\beta}$ (V)	$\rho^{\alpha-\beta}$ (C)	$\rho^{\alpha-\beta}$ (C$_{ipso}$)	$\rho^{\alpha-\beta}$ (C$_{para}$)	$\rho^{\alpha-\beta}$ (B)	$\langle S^2 \rangle$
BP86	1.234	−0.028	−0.021	−0.017	0.019	0.772
B3LYP	1.298	−0.032	−0.027	−0.018	0.015	0.791
B30LYP	1.365	−0.037	−0.033	−0.022	0.015	0.811
B35LYP	1.392	−0.039	−0.035	−0.024	0.016	0.821
B40LYP	1.460	−0.046	−0.040	−0.027	0.017	0.847
BHLYP	1.588	−0.057	−0.051	−0.033	0.018	0.911

question of whether the decrease of a_{iso}(^{51}V) with increased tilt angle α is due to delocalization of the SOMO, to valence-shell spin polarization, or to changes in core−shell spin-polarization contributions at the vanadium atom. As transition-metal hyperfine couplings and the delocalization of spin between metal and ligand are known to be very sensitive to the quality of the exchange-correlation functional in DFT calculations,[38] we compare various hybrid functionals with different admixtures of exact (Hartree−Fock) exchange.

Spin-Density Analysis. As the computed EPR parameters are critically dependent on the spin-density distribution, Table 3 provides Mulliken atomic spin densities obtained with different exchange-correlation functionals for [V(η^6-C$_6$H$_5$)$_2$BN(SiMe$_3$)$_2$] (**1**), which is the most tilted complex. Table 4 shows the Mulliken atomic spin densities obtained with the B3LYP

functional for various vanadium complexes, and spin-density isosurface plots are shown in Figure 9f.

For [V(η^6-C$_6$H$_5$)$_2$BN(SiMe$_3$)$_2$] (**1**), Table 3 shows a larger spin density at vanadium than the formally expected single unpaired spin. Significant spin polarization is found for the carbon atoms of the benzene ligand (giving negative spin density). When going from the BP86 GGA functional to hybrid functionals with increasing Hartree−Fock exchange admixture, an increase of the spin density at vanadium is accompanied by more negative spin densities on the ligand carbon atoms (Table 3). While the enhanced spin density at vanadium does to some extent reflect an increase in metal−ligand bond ionicity by exact-exchange admixture (confirmed by population analyses), known to diminish the self-interaction errors present at LDA and GGA levels,[39] the negative spin densities on carbon suggest that a main effect of the exact-exchange admixture is an enhancement of spin polarization across the metal−ligand bond.[40] This accumulates even more positive spin density at vanadium. Furthermore, the larger spin contamination is known to be related to an enhancement of valence-shell spin polarization by exact-exchange admixture for transition-metal complexes.[38] These observations are all consistent with strong metal−ligand covalency.

This spin polarization is analyzed more closely for the parent sandwich complex [V(η^6-C$_6$H$_6$)$_2$] and the strongly bent complex **1** in Figure 8. The SOMO spin density itself exhibits essentially no delocalization onto the ligand for **1** and relatively little for [V(η^6-C$_6$H$_6$)$_2$]. The spin polarization of the doubly occupied MOs by the SOMO is clearly responsible for (a) enhanced positive spin density on vanadium and (b) appreciably negative spin density on the arene carbon atoms. This indicates already that SOMO delocalization alone does not account for the main trends in the distribution of spin density between the metal and the ligands.

The Mulliken spin density on vanadium is indeed significantly larger than 1.0 for all low-spin d^5-vanadium(0) complexes studied here (Table 4), and a significant spin polarization of the carbon atoms of the benzene ligand is also apparent (Table 4 and Supporting Information). The vanadium spin density is slightly greater for complexes with a larger tilt angle α (**1**, **4**) than for those complexes with a smaller tilt angle α (**6**, **10**). However, complex **5** with a medium tilt angle α has the highest spin density at vanadium. There is little difference in the spin-

(38) (a) Munzarová, M.; Kaupp, M. *J. Phys. Chem. A* **1999**, *103*, 9966. (b) Munzarová, M.; Kubácek, P.; Kaupp, M. *J. Am. Chem. Soc.* **2000**, *122*, 11900.

(39) Furche, F.; Perdew, J. P. *J. Chem. Phys.* **2006**, *124*, 044103/1.

(40) (a) Remenyi, C.; Kaupp, M. *J. Am. Chem. Soc.* **2005**, *127*, 11399. (b) Remenyi, C.; Reviakine, R.; Kaupp, M. *J. Phys. Chem. B* **2007**, *111*, 8290.

Table 4. Mulliken Atomic Spin Densities and $\langle S^2 \rangle$ Expectation Values (B3LYP)

	α_{calcd} (deg)	$\rho^{\alpha-\beta}$ (V)	$\rho^{\alpha-\beta}$ (C$_{ar}$)^a	$\rho^{\alpha-\beta}$ (C$_{ipso}$)	$\rho^{\alpha-\beta}$ (C$_{para}$)	$\rho^{\alpha-\beta}$ (X)^b	$\langle S^2 \rangle$
[V(η^6-C$_6$H$_5$)$_2$BN(SiMe$_3$)$_2$] (**1**)	30.6	1.298	−0.032	−0.027	−0.018	0.015	0.791
[V(η^6-C$_6$H$_5$)$_2$BN^{i}Pr$_2$] (**4**)	30.1	1.300	−0.032	−0.027	−0.019	0.015	0.791
[V(η^6-C$_6$H$_5$)$_2$SiMe^{i}Pr] (**2**)	20.9	1.294	−0.030	−0.021	−0.024	−0.005	0.788
[V(η^6-C$_6$H$_5$)$_2$B$_2$(NMe$_2$)$_2$] (**5**)	13.8	1.303	−0.030	−0.025	−0.031	−0.001	0.789
[(η^6-C$_6$H$_6$)V(η^6-C$_6$H$_5$B(Ph)N(SiMe$_3$)$_2$] (**7**)	5.3	1.300	−0.032	−0.028	−0.043	−0.013	0.783
[V(η^6-C$_6$H$_5$)$_2$Si$_2$Me$_4$] (**6**)	5.2	1.288	−0.030	−0.026	−0.029	0.003	0.786
[V(η^6-C$_6$H$_5$BNMe$_2$)C(Me)C(Me)(η^6-C$_6$H$_5$BNMe$_2$)] (**10**)	2.1	1.280	−0.029	−0.035	−0.029	0.001	0.790
[V(η^6-C$_6$H$_5$)$_2$]	0.0	1.283	−0.031				0.784

^{a} C$_{ar}$ is the average of all carbon atoms of the benzene ligand. ^{b} X is the bridging atom B or Si.
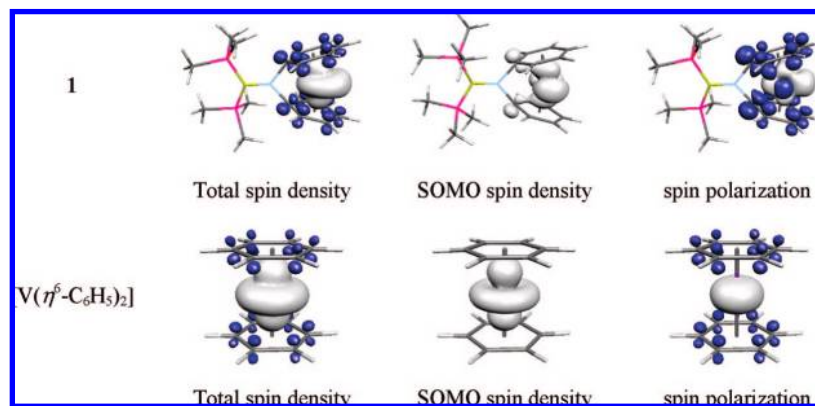
Figure 8. Influence of spin polarization in [V(η^6-C$_6$H$_5$)$_2$BN(SiMe$_3$)$_2$] (**1**) and [V(η^6-C$_6$H$_5$)$_2$]. Spin-density isosurfaces ±0.002 au (B3LYP).
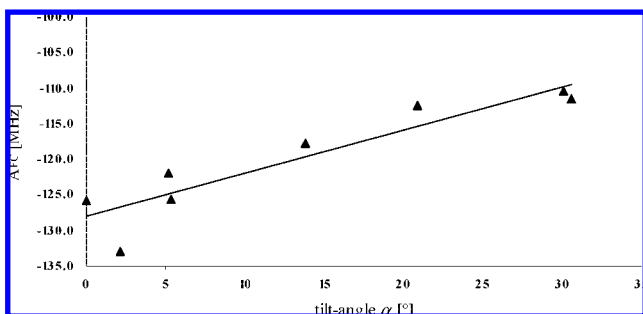
Figure 9. Plot of the Fermi contact contribution A_{FC} to $a_{iso}(^{51}V)$ vs tilt angle α.

density distribution on the C$_{ipso}$ atoms, as well as for the averaged spin density of the arene carbon atoms for the different complexes. A larger negative spin density on the C$_{para}$ atoms for smaller tilt angles is observed. Therefore, the spin density alone does not provide conclusive answers about the origin of the $a_{iso}(^{51}V)$-α correlation. A closer analysis of the hyperfine coupling itself is required.

^{51}V Hyperfine Coupling Constants. The available experimental anisotropic as well as isotropic ^{51}V hyperfine data are compared to the DFT results with three different hybrid functionals in Table 5 (a more complete comparison for more gradient-corrected and hybrid functionals is provided in the Supporting Information). The experimentally observed trends from axial symmetry for [V(η^6-C$_6$H$_6$)$_2$] to a clearly rhombic hyperfine tensor for the ansa complexes (**1**, **2**, **4**–**7**, **10**) are confirmed by the calculations. The anisotropic part of the hyperfine coupling tensors depends less on exact-exchange admixture than the isotropic couplings. The coupling anisotropies are overestimated somewhat already at gradient-corrected BP86 level. As the computed anisotropies decrease slightly further upon exact-exchange admixture, agreement with experiment becomes also somewhat worse. The isotropic coupling

constant a_{iso} in such systems depends much more on exact-exchange admixture, partly due to an enhancement of (overall negative) core−shell spin-polarization contributions to the spin density at the nucleus[38,41] (and due to generally more spin density on vanadium). This renders the couplings more negative and improves agreement with the experimental data up to a certain value of the exact-exchange mixing coefficient a_0 (the "best" functionals are compared in Table 5). All $a_{iso}(^{51}$V) computed with the B30LYP and B35LYP functionals are within 8.3% of experiment, where available. B30LYP results are not quite negative enough, whereas B35LYP results are slightly too negative; that is, these two levels bracket the experimental isotropic couplings. The sign of a_{iso} was not determined experimentally but is strongly suggested to be negative in all cases by the computations.

In general, relativistic effects on hyperfine coupling constants are important for transition-metal complexes. A second-order perturbation treatment[42] gave significant spin−orbit contributions to the A tensor, given separately as contributions to the isotropic couplings ("pseudocontact" couplings, A_{PC}) and to the anisotropic part ($A_{ii}^{dip,2}$). The pseudocontact contributions amount to ca. 7−11% of the nonrelativistic isotropic A_{FC} values and become more negative with more exact exchange.

While 30−35% exact-exchange admixture gave the best absolute agreement with experimental isotropic couplings, the B3LYP functional with 20% exact exchange was chosen for further analysis. The reason was the less pronounced spin contamination and the better reproduction of the experimental differences between Fermi contact contributions for different complexes at this level. Our calculations confirm the experi-

(41) Malkin, V. G.; Malkina, O. L.; Casida, M. E.; Salahub, D. R. *J. Am. Chem. Soc.* **1994**, *116*, 5898.
(42) (a) Arbouznikov, A. V.; Vaara, J.; Kaupp, M. *J. Chem. Phys.* **2004**, *120*, 2127. (b) Remenyi, C.; Reviakine, R.; Arbuznikov, A. V.; Vaara, J.; Kaupp, M. *J. Phys. Chem. A* **2004**, *108*, 5026.

Table 5. Computed and Experimental ^{51}V HFC Tensors (MHz)[a]

		a_{iso}[a]	A_{11}, A_{22}, A_{33}	A_{FC}	A_{PC}	T_{11}, T_{22}, T_{33}	$A_{11}^{dip,2}, A_{22}^{dip,2}, A_{33}^{dip,2}$	$\langle S^2 \rangle$
1	B3LYP	−123.3	−88.5	−111.6	−11.7	−83.3	−16.8	0.791
			−49.0			−45.4	−15.2	
			137.5			128.7	−2.8	
	B30LYP	−151.1	−83.4	−138.1	−13.0	−78.1	−18.2	0.811
			−46.6			−42.9	−16.6	
			130.0			121.1	−4.0	
	B35LYP	−163.8	−81.3	−150.1	−13.7	−76.0	−18.9	0.821
			−45.5			−41.9	−17.3	
			126.9			117.9	−4.7	
	expt	|152.0|	|93.0|				
			|55.2|					
			|147.8|					
4	B3LYP	−122.2	−88.9	−110.5	−11.7	−83.7	−16.9	0.791
			−48.9			−45.3	−15.3	
			137.9			129.0	−2.8	
	B30LYP	−147.5	−85.5	−134.6	−12.9	−80.2	−18.2	0.806
			−47.6			−43.9	−16.5	
			133.1			124.1	−3.8	
	B35LYP	−163.0	−81.7	−149.2	−13.8	−76.4	−19.1	0.821
			−45.4			−41.7	−17.4	
			127.1			118.1	−4.7	
	expt	|154.0|	|96.0|				
			|54.0|					
			|149.8|					
2	B3LYP	−123.9	−80.9	−112.5	−11.4	−76.1	−16.2	0.788
			−62.3			−58.3	−15.5	
			143.2			134.4	−2.7	
	B30LYP	−148.5	−77.8	−135.9	−12.6	−73.0	−17.4	0.801
			−60.6			−56.5	−16.6	
			138.5			129.5	−3.6	
	B35LYP	−163.4	−74.7	−150	−13.4	−69.9	−18.2	0.814
			−58.4			−54.3	−17.4	
			133.1			124.2	−4.4	
	expt	|157.6|	|91.6|				
			|74.8|					
			|166.0|					
5	B3LYP	−129.0	−75.0	−117.7	−11.3	−70.2	−16.0	0.789
			−67.6			−63.6	−15.3	
			142.6			133.9	−2.6	
	B30LYP	−153.3	−72.2	−140.9	−12.4	−67.4	−17.2	0.803
			−65.2			−61.1	−16.4	
			137.4			128.5	−3.5	
	B35LYP	−170.7	−67.8	−157.5	−13.2	−63.0	−18.0	0.822
			−61.2			−57.2	−17.3	
			129.0			120.2	−4.5	
	expt	|164.4|	|84.8|				
			|76.4|					
			|161.6|					
7	B3LYP	−137.0	−81.6	−125.6	−11.4	−76.9	−16.0	0.783
			−61.3			−57.1	−15.5	
			142.9			134.0	−2.5	
	B30LYP	−165.3	−75.6	−152.6	−12.7	−70.9	−17.3	0.814
			−56.9			−52.7	−16.9	
			132.5			123.6	−3.7	
	B35LYP	−181.1	−71.7	−167.6	−13.5	−67.1	−18.1	0.832
			−53.9			−49.7	−17.8	
			125.6			116.7	−4.6	
	expt	|173.0|	|95.2|				
			|73.4|					
			|168.8|					
6	B3LYP	−133.2	−73.2	−122.0	−11.2	−68.9	−15.6	0.786
			−71.4			−66.9	−15.7	
			144.6			135.8	−2.5	
	B30LYP	−156.6	−71.0	−144.3	−12.3	−66.6	−16.7	0.798
			−69.1			−64.5	−16.8	
			140.1			131.2	−3.3	
	B35LYP	−170.9	−68.5	−157.9	−13.0	−64.1	−17.4	0.810
			−66.5			−61.9	−17.6	
			135.0			126.0	−4.0	
	expt	|170.8|	|84.0|				
			|84.0|					
			|168.0|					
10	B3LYP	−133.1	−83.9	−122.0	−11.1	−79.2	−15.8	0.790
			−63.4			−59.4	−15.1	
			147.3			138.6	−2.4	
	B30LYP	−159.8	−78.9	−147.5	−12.3	−74.2	−17.0	0.802
			−59.7			−55.7	−16.3	
			138.6			129.8	−3.5	
	B35LYP	−174.9	−75.4	−161.8	−13.1	−70.7	−17.8	0.816
			−56.9			−52.9	−17.1	
			132.3			123.6	−4.3	
	expt	|172.8|	|94.6|				
			|75.6|					
			|170.0|					

Table 5. Continued

		$a_{\mathrm{iso}}{}^a$	A_{11}, A_{22}, A_{33}	A_{FC}	A_{PC}	T_{11}, T_{22}, T_{33}	$A_{11}{}^{\mathrm{dip},2}, A_{22}{}^{\mathrm{dip},2}, A_{33}{}^{\mathrm{dip},2}$	$\langle S^2 \rangle$
BBV[b]	B3LYP	−136.9	−72.7	−125.9	−11.0	−68.3	−15.3	0.784
			−72.3			−67.9	−15.3	
			144.9			136.3	−2.3	
	B30LYP	−159.7	−70.5	−147.7	−12.0	−66.1	−16.4	0.795
			−70.2			−66.0	−16.4	
			140.8			131.9	−3.1	
	B35LYP	−173.6	−68.1	−160.9	−12.7	−63.6	−17.1	0.805
			−67.8			−63.4	−17.1	
			135.9			127.0	−3.8	

[a] a_{iso} is the total isotropic value, A_{ii} represents the traceless part of the full A tensor, A_{FC} and A_{PC} denote the isotropic first-order Fermi contact and second-order pseudocontact (spin−orbit) contributions to the full total A tensor, respectively. T_{ii} and $A_{ii}{}^{\mathrm{dip},2}$ denote, respectively, the first-order nonrelativistic and second-order spin−orbit anisotropic tensors. [b] BBV = [V(η^6-C₆H₆)₂].

Table 6. Orbital Contributions to $A_{\mathrm{FC}}(V)$ (MHz)[a]

|	α_{calcd} (deg)	A_{FC}	1s	2s	3s	total CS[b]	VS spin polarization[c]	SOMO[d]	total VS[e]
1	30.6	−111.6	−4.7	−381.5	133.7	−252.4	104.7	36.0	140.8
4	30.1	−110.5	−4.6	−382.4	134.1	−252.9	104.1	38.3	142.4
2	20.9	−112.5	−4.2	−381.9	131.8	−254.3	92.0	49.8	141.8
5	13.8	−117.7	−4.0	−383.2	129.5	−257.6	92.8	47.1	139.9
7	5.3	−125.6	−3.9	−382.8	127.9	−258.7	89.7	43.5	133.1
6	5.2	−122.0	−3.9	−381.6	128.0	−257.4	89.3	46.1	135.4
10	2.1	−122.0	−3.8	−375.9	125.6	−254.2	90.5	41.7	132.2
BBV[f]	0	−125.9	−3.8	−378.0	124.9	−257.0	89.3	41.9	131.1

[a] B3LYP results. [b] Sum of core−shell spin-polarization contributions (from 1s, 2s, and 3s shells). [c] Sum of valence-shell spin-polarization contributions. [d] SOMO contribution. [e] Sum of valence-shell spin-polarization and SOMO contributions. [f] BBV = [V(η^6-C₆H₆)₂].

mentally observed correlation: Lower coupling constants $a_{\mathrm{iso}}(^{51}V)$ correspond overall to smaller tilting angles α (Table 6 and Figure 9).

Since the dependence of $a_{\mathrm{iso}}(^{51}V)$ on the degree of tilting is a key aspect here, the Fermi contact term of $a_{\mathrm{iso}}(^{51}V)$, which is the dominant contribution to the isotropic hyperfine couplings, was broken down into molecular orbital contributions (Table 6). Often variations in core−shell spin-polarization contributions, caused by changes in d-populations, are responsible for trends in isotropic metal hyperfine couplings.[38] However, in the present series, the sum of the core−shell (1s, 2s, and 3s) contributions to A_{FC} varies relatively little. The variation of only ca. 4 MHz is clearly too small to explain the total variation of $a_{\mathrm{iso}}(V)$ by almost 20 MHz.

The main variation must thus come either from the direct SOMO contribution to the spin density at the vanadium nucleus or from spin polarization of the doubly occupied valence orbitals. Table 6 shows that both aspects are of importance: When comparing the virtually parallel sandwich complexes [V(η^6-C₆H₆)₂] and **10** with the most tilted species **1** and **4**, it is clear that more positive VS spin-polarization contributions are responsible for the less negative hyperfine couplings. In fact, the SOMO contribution is somewhat *less positive* for the strongly tilted **1** and **4** and compensates essentially only the 5 MHz less negative core−shell contributions. Here obviously spin polarization dominates. Matters become a bit more complicated for the intermediately tilted species **2** and **5**: of the 8−13 MHz less negative A_{FC} compared to [V(η^6-C₆H₆)₂] or **10**, only ca. 3 MHz is caused by somewhat larger VS spin-polarization contributions. The SOMO contribution in these two complexes appears to be increased by ca. 5−8 MHz.
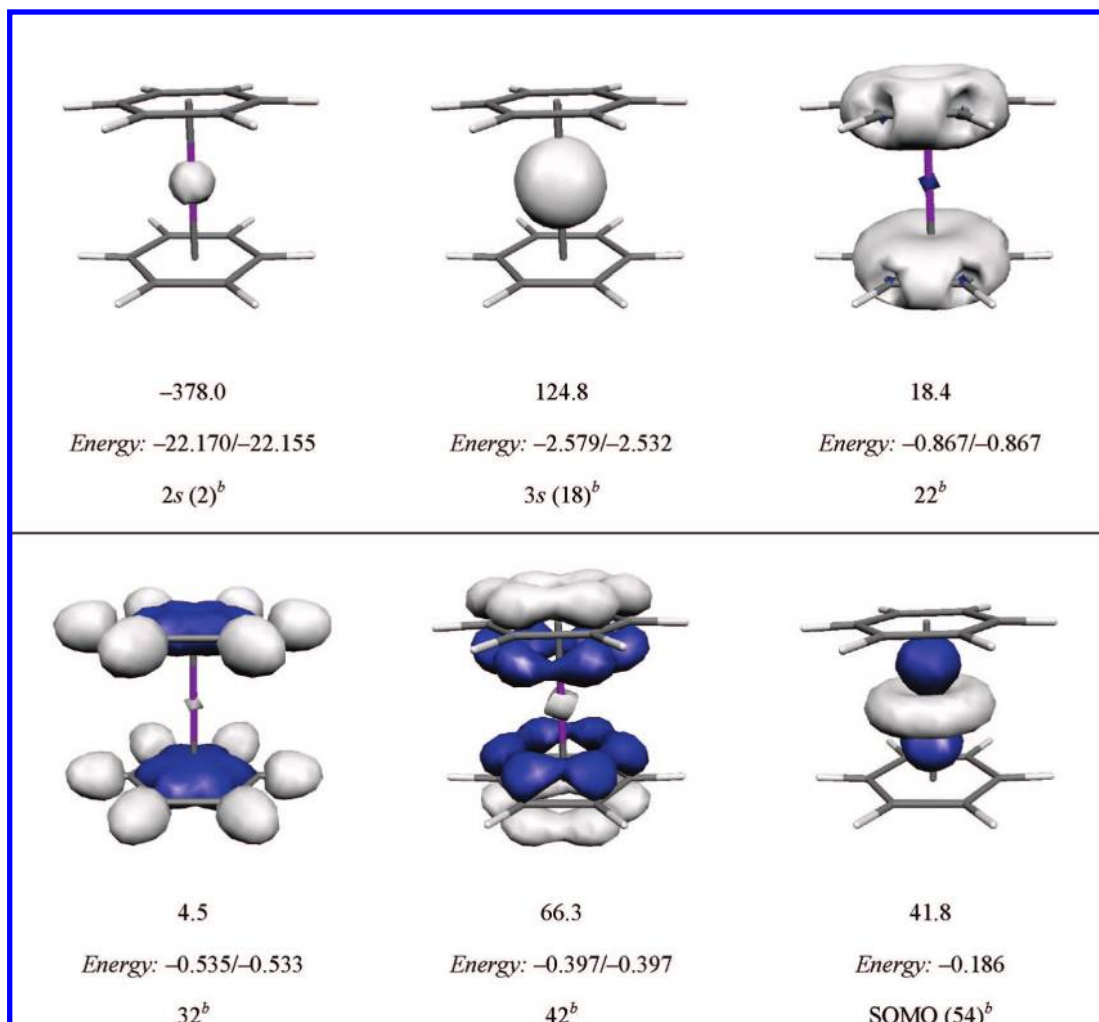
Figure 10 shows that the lower SOMO contributions are indeed due to enhanced spin delocalization: The vanadium character of the SOMO decreases somewhat. This is consistent with general notions of orbital delocalization in bent sandwich complexes.[43] In the literature, the reduction of $|a_{\mathrm{iso}}(V)|$ upon bending of the η^6-(arene)₂M units was ascribed to this enhanced delocalization of the SOMO.[21−23,31] Obviously, our analyses
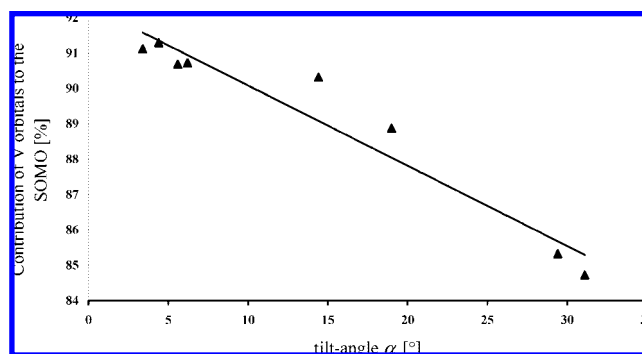
Figure 10. Character of the SOMO as function of tilt angle α.

show that the effect of SOMO delocalization alone is too small, and partly of the wrong sign (see above), to explain the observed trends for the series of complexes studied here.

The obviously crucial influence of valence-shell spin polarization is more difficult to analyze, as it may arise from quite a number of valence MOs. In the symmetrical complex [V(η^6-C₆H₆)₂] (Table 7), only three sets of doubly occupied valence orbitals contribute significantly to the spin density at the vanadium nucleus and thus to $A_{\mathrm{FC}}(V)$, with the metal−ligand σ-antibonding MO 42 being clearly dominant (Table 7).

Matters are much more complicated for less symmetrical, bent complexes such as **1** (Table 8). Now the valence-shell spin-polarization contributions are distributed over a much larger number of MOs. While MOs 22 and 32 in [V(η^6-C₆H₆)₂] reappear with only slight changes in their contributions (now MOs 40 and 57, respectively, in **1**; Table 8), the dominant contribution of MO 42 in [V(η^6-C₆H₆)₂] (Table 7) is now spread over about 14 MOs. As contributions from MOs 61−75 (Table 7) are small and almost cancel, we may concentrate on the six MOs 76, 78, 80, 86, 95, and 98. Their contributions add up to 81.1 MHz compared to 66.3 MHz of MO 42 in [V(η^6-C₆H₆)₂], thus explaining the ca. 15 MHz difference in $A_{\mathrm{FC}}(V)$ (cf. Tables 3 and 6). Closer examination of the MO energies (Tables 7 and

Table 7. Significant Orbital Contributions (>2 MHz) to $A_{FC}(V)$ for $[V(\eta^6\text{-}C_6H_5)_2]$ (MHz);[a,b] Energies Are in Atomic Units

−378.0	124.8	18.4
Energy: −22.170/−22.155	*Energy: −2.579/−2.532*	*Energy: −0.867/−0.867*
2s (2)[b]	3s (18)[b]	22[b]
4.5	66.3	41.8
Energy: −0.535/−0.533	*Energy: −0.397/−0.397*	*Energy: −0.186*
32[b]	42[b]	SOMO (54)[b]

[a] B3LYP results. [b] Orbital number.

8) indicates that, while MO 42 in $[V(\eta^6\text{-}C_6H_6)_2]$ is at −0.397 a.u., the six MOs in question for **1** are spread over a range of MO energies between −0.4 and −0.15 a.u. (Table 8). The tilting of the π-coordinated rings thus obviously destabilizes some key valence MOs. As valence-shell spin polarization tends to be more pronounced for MOs of high energy,[38] this destabilization of valence MOs by tilting of the sandwich complex is the likely explanation for the enhanced valence-shell spin-polarization contributions in the significantly bent systems (cf. Table 6), and thus for the overall less negative $A_{FC}(V)$ in these cases.

Summary and Conclusions

In this article, the derivatization of the paramagnetic sandwich complex $[V(\eta^6\text{-}C_6H_6)_2]$ to afford [*n*]vanadoarenophanes (*n* = 1−2) with boron and silicon in bridging positions was described. These species were prepared by convenient salt-elimination reactions of the selectively 1,1′-dilithiated sandwich precursor with appropriate element dihalides. An optimized procedure for the dimetalation of bis(benzene)vanadium employing BuLi in the presence of tmeda at slightly elevated temperatures allowed for the isolation and characterization of $[V(\eta^6\text{-}C_6H_5Li)_2]\cdot$tmeda (**3**·tmeda). The selectivity of the dimetalation was confirmed by X-ray diffraction of its thf solvate $[V(\eta^6\text{-}C_6H_5Li)_2]\cdot$(thf)$_7$

(**3**·thf), which proved to be isostructural to its chromium congener and thus features a dimeric structure in the solid state. Structural characterization of metalated sandwich complexes is still a challenging area owing to the high reactivity of these species, and hence, the solution of the molecular structure of **3** contributes to the understanding of the fundamentals that determine the conformation of this class of organometallic compounds. Starting from this, novel [1]- (**4**) and [2]bora (**5**), as well as the related [2]silavanadoarenophanes (**6**) were synthesized and fully characterized. X-ray diffraction studies revealed the presence of ring strain to a greater or lesser extent depending on the number and covalent radii of the bridging elements. In addition, the reactivity of the diborane-bridged derivative **5** toward low-valent transition metals was intensively studied. It was shown that **5** serves as a facile diborane(4) precursor in diboration reactions with 2-butyne to afford the *ansa*-bis(boryl)alkene **10** under stoichiometric, homogeneous ($[Pt(PEt_3)_3]$), and heterogeneous (Pd/C) catalytic conditions. The proposed intermediate **9**, the product of the oxidative addition of the B−B bond to the Pt center of $[Pt(PEt_3)_3]$, was also isolated. As expected, the driving force of this transformation is given by the reduction of molecular ring strain, which was
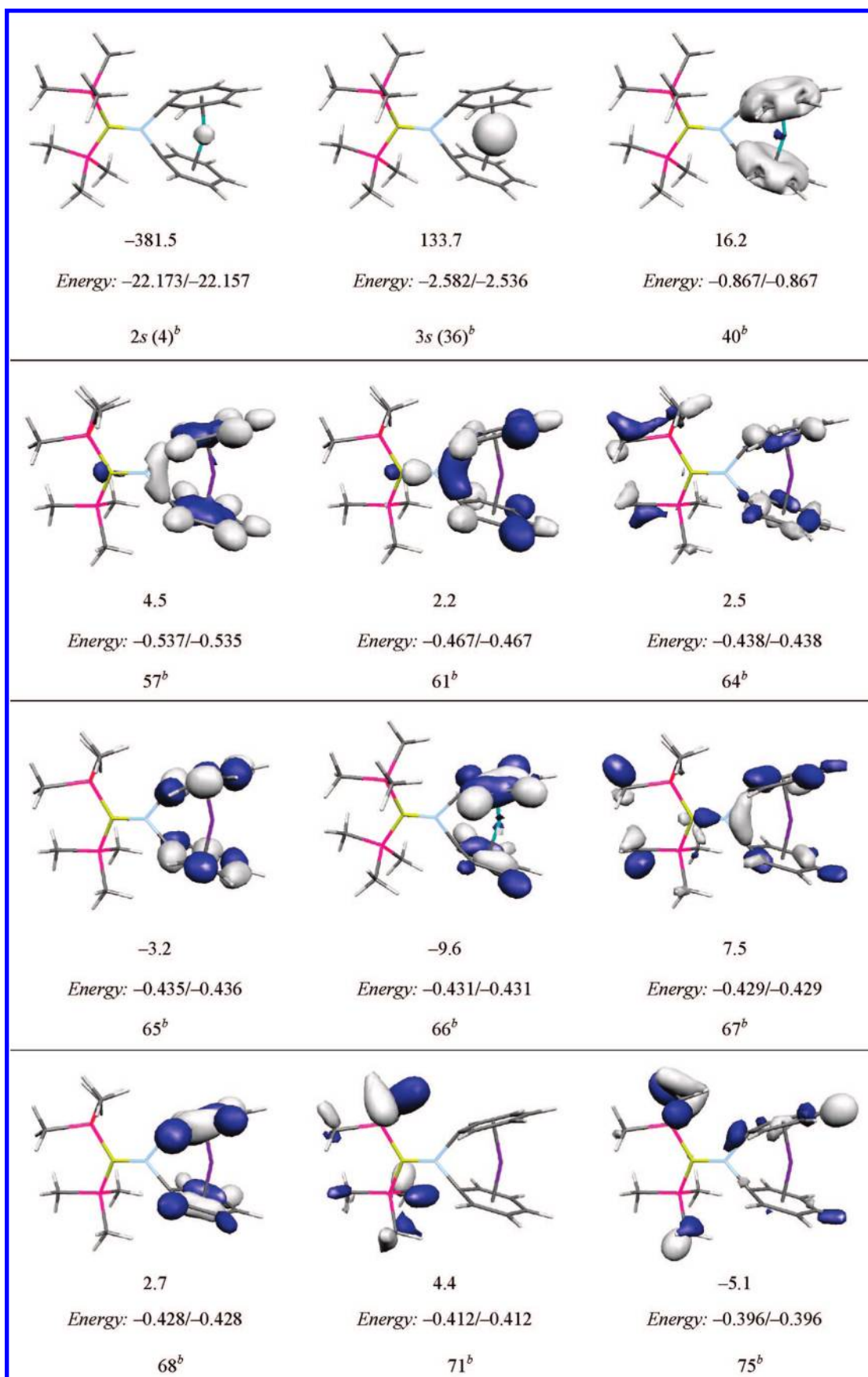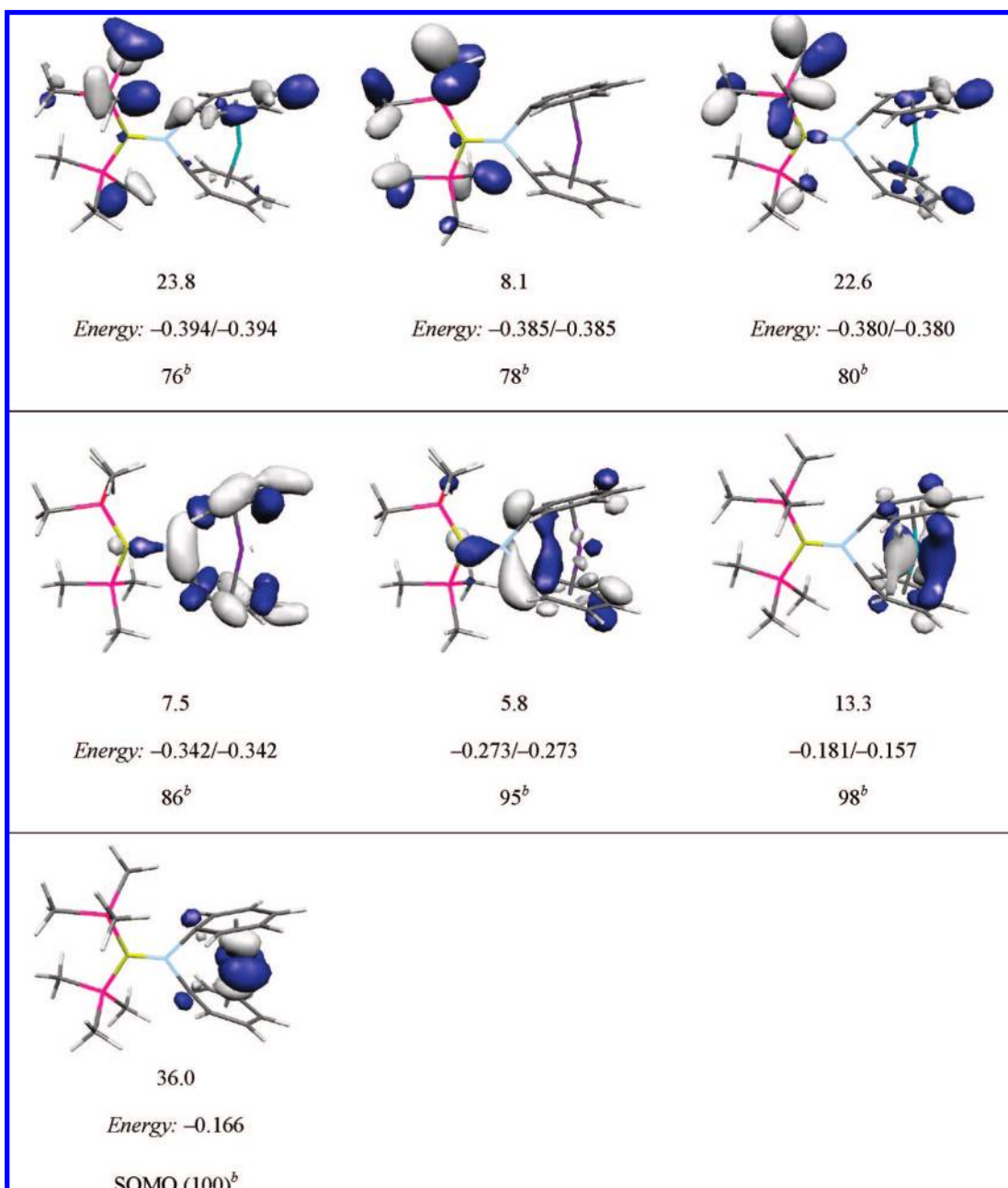
Table 8. Significant MO Contributions (>2 MHz) to $A_{FC}(V)$ for $[V(\eta^6\text{-}C_6H_5)_2BN(SiMe_3)_2]$ (MHz);[a,b] Energies Are in Atomic Units

Table 8. Continued

23.8

Energy: −0.394/−0.394

76[b]

8.1

Energy: −0.385/−0.385

78[b]

22.6

Energy: −0.380/−0.380

80[b]

7.5

Energy: −0.342/−0.342

86[b]

5.8

−0.273/−0.273

95[b]

13.3

−0.181/−0.157

98[b]

36.0

Energy: −0.166

SOMO (100)[b]

[a] B3LYP results. [b] Orbital number.

confirmed by a gradual decrease of the tilt angle α in **5**, **9**, and **10**, respectively.

The electronic structure of these species, as well as of the previously described derivatives **1**, **2**, and **7**, was investigated by means of UV−vis spectroscopy and EPR spectroscopy. Whereas the UV−visible spectra did not reveal any distinct details, the EPR spectra showed an obvious correlation between the degree of molecular distortion and the observed hyperfine coupling constants a_{iso}. State-of-the-art DFT calculations of the hyperfine tensors reproduce the experimentally observed trends and allowed a closer analysis of this type of dependence. Spin−orbit contributions to the hyperfine couplings are non-negligible and clearly have to be included for a quantitative description. However, the trend with tilt angle is dominated by the nonrelativistic Fermi contact term, which was subsequently

broken down into molecular orbital contributions. Core−shell spin-polarization contributions vary little, and it is the spin polarization of doubly occupied valence orbitals around the vanadium center that provides the dominant contribution to the observed trend in $a_{iso}(V)$. Closer analysis suggests that a larger tilt angle α destabilizes a number of key valence orbitals, making them more amenable to being spin-polarized by the SOMO. Their contribution to $a_{iso}(V)$ becomes more positive upon tilting, thereby rendering the overall coupling constant less negative. The direct SOMO contributions vary too little (and partly in the wrong direction) to explain the observed dependence.

Experimental Section

General Remarks. All manipulations were performed under an inert atmosphere of dry argon using standard Schlenk techniques

or in a glovebox. Solvents were dried according to standard procedures, freshly distilled before use, degassed, and stored under argon over activated molecular sieves. $[V(\eta^6\text{-}C_6H_6)_2]$,[44] $Cl_2BN^iPr_2$,[45] $(NMe_2)ClB\text{-}BCl(NMe_2)$,[46] and $[Pt(PEt_3)_3]$[47] were prepared according to known methods. $Me_2ClSi\text{-}SiClMe_2$ was obtained from Aldrich and distilled from magnesium turnings before use. BuLi was purchased from Aldrich as 1.6 mol L^{-1} solutions in hexanes. Tmeda was dried over potassium and distilled under argon before use. All other chemicals were obtained commercially and were used without further purification. The NMR spectra were recorded on a Bruker Avance 200 (^{1}H: 200.13 MHz, ^{11}B: 64.29 MHz) FT-NMR spectrometer. ^{1}H NMR spectra were referenced to external TMS via the residual protons of the solvent. ^{11}B{^{1}H} NMR spectra were referenced to BF$_3$·OEt$_2$. UV–vis spectra were recorded on a Shimadzu UV Mini 1240 UV–vis photometer. Microanalyses for C, H, and N were performed on a Leco CHNS-932 elemental analyzer. Mass spectra were recorded on a Finnigan MAT-8200 spectrometer (EI, 70 eV). EPR spectra were recorded on a Bruker ESP300E X-band spectrometer with a Hewlett-Packard 5350B microwave frequency counter. The field calibration was checked by measuring the resonance of the diphenylpicrylhydrazyl (dpph) radical before each series of spectra. Spectra were simulated using the Bruker Simfonia program.

$[V(\eta^6\text{-}C_6H_5Li)_2]$·tmeda, 3·tmeda. A solution of $[V(\eta^6\text{-}C_6H_6)_2]$ (1.00 g, 4.83 mmol) in heptane was treated with tmeda (1.40 g, 12.07 mmol) and BuLi (7.54 mL, 12.07 mmol) at room temperature (RT) and heated to 80 °C over a period of 16 h. The resulting reddish-brown precipitate was collected by filtration, washed with pentane (3 × 5 mL), and subsequently dried in vacuo to afford $[V(\eta^6\text{-}C_6H_5Li)_2]$·tmeda (3·tmeda) (1.38 g, 4.10 mmol, 85%) as a brown powder. Anal. Calcd (%) for C$_{18}$H$_{26}$Li$_2$N$_2$V (335.24): C, 64.49; H, 7.82; N, 8.36. Found: C, 65.11; H, 8.01; N, 7.99.

$[V(\eta^6\text{-}C_6H_5)_2BN^iPr_2]$, 4. A slurry of $[V(\eta^6\text{-}C_6H_5Li)_2]$·tmeda (3·tmeda) (0.35 g, 1.04 mmol) in heptane (20 mL) was cooled to −78 °C and treated dropwise over a period of 3 h with a solution of $Cl_2BN^iPr_2$ (0.19 g, 1.04 mmol) in heptane (4 mL). After complete addition, the reaction mixture was allowed to reach ambient temperature. During this time, the color of the suspension turned from pale brown to deep-red and an off-white precipitate deposited. After the solid had settled, the solution was filtered into another flask by a filter canula and the filtrate was concentrated to about 4 mL in volume. Cooling to −60 °C afforded 4 as a dark-red, microcrystalline solid, which was subsequently isolated after washing with cold pentane (3 × 2 mL, −100 °C) and drying in vacuo (0.22 g, 0.70 mmol, 67%). EPR (toluene, 110 K): ⟨g⟩ = 1.983; ⟨a⟩ (^{51}V) = 55.0 G. MS (EI): m/z (%) = 316 (17) [M$^+$], 250 (47) [M$^+$ − V − Me], 217 (18) [M$^+$ − N^{i}Pr$_2$], 105 (100) [M^{3+}], 43 (12) [^{i}Pr$^+$]. λ_{max} (ε) = 416 nm (2753 L mol^{-1} cm^{-1}). Anal. Calcd (%) for C$_{18}$H$_{24}$BNV (316.14): C, 68.39; H, 7.65; N, 4.43. Found: C, 68.19; H, 7.53; N, 4.63.

$[V(\eta^6\text{-}C_6H_5)_2B_2(NMe_2)_2]$, 5. A slurry of $[V(\eta^6\text{-}C_6H_5Li)_2]$·tmeda (3·tmeda) (0.42 g, 1.25 mmol) in heptane (25 mL) was treated dropwise at −78 °C with a solution of $(NMe_2)ClB\text{-}BCl(NMe_2)$ (0.23 g, 1.25 mmol) in heptane (10 mL). After 2 h, the reaction mixture was allowed to reach ambient tempertaures and was further stirred for 14 h at RT. All volatiles were removed in vacuo, and the black residue was extracted with pentane (2 × 10 mL). After removal of all insolubles by filtration, the black filtate was reduced to 5 mL in volume and stored at −70 °C to yield $[V(\eta^6\text{-}C_6H_5)_2B_2(NMe_2)_2]$ (5) (0.17 g, 0.54 mmol, 43%), which was isolated as a black amorphous solid after being washed with cold pentane (1 × 2 mL, −100 °C). EPR (toluene, 130 K): ⟨g⟩ = 1.985; ⟨a⟩ (^{51}V) = 58.7 G. MS (EI): m/z (%) = 315 (52) [M$^+$], 272 (21)

[M$^+$ − NMe$_2$], 263 (84) [M$^+$ − V], 249 (47) [M$^+$ − V − Me], 132 (74) [PhBNMe$_2^+$], 91 (100) [C$_7$H$_7^+$], 44 (33) [NMe$_2^+$]. λ_{max} (ε) = 460 nm (2437 L mol^{-1} cm^{-1}). Anal. Calcd (%) for C$_{16}$H$_{22}$B$_2$N$_2$V (314.92): C, 61.02; H, 7.04; N, 8.90. Found: C, 61.21; H, 6.94; N, 8.63.

$[V(\eta^6\text{-}C_6H_5)_2Si_2Me_4]$, 6. A suspension of $[V(\eta^6\text{-}C_6H_5Li)_2]$·tmeda (3·tmeda) (0.35 g, 1.04 mmol) in heptane (15 mL) was cooled to −78 °C and treated dropwise with a solution of $Me_2ClSi\text{-}SiClMe_2$ (0.20 g, 1.04 mmol) in heptane (5 mL). After 2 h, the reaction mixture was allowed to reach ambient temperature and was stirred at RT over a period of 20 h. After removal of all insolubles by filtration, the black filtrate was reduced to 5 mL in volume. Crystallization at −30 °C afforded $[V(\eta^6\text{-}C_6H_5)_2Si_2Me_4]$ (6) (0.24 g, 0.75 mmol, 72%) as a black, microcrystalline solid, which was isolated after being washed with cold pentane (3 × 2 mL, −100 °C) and drying in vacuo. EPR (toluene, 110 K): ⟨g⟩ = 1.984; ⟨a⟩ (^{51}V) = 61.0 G. MS (EI): m/z (%) = 321 (100) [M$^+$], 270 (10) [M$^+$ − V], 263 (42) [M$^+$ − SiMe$_2$], 197 (18) [Ph$_2$SiMe$^+$], 135 (75) [PhSiMe$_2^+$], 51 (23) [V$^+$]. λ_{max} (ε) = 467 nm (1671 L mol^{-1} cm^{-1}). Anal. Calcd (%) for C$_{16}$H$_{22}$Si$_2$V (321.46): C, 59.78; H, 6.90. Found: C, 59.50; H, 6.81.

$[V(\eta^6\text{-}C_6H_5BNMe_2)Pt(PEt_3)_2(\eta^6\text{-}C_6H_5BNMe_2)]$, 9. A resealable Schlenk flask equipped with a Teflon valve was charged with $[V(\eta^6\text{-}C_6H_5)_2B_2(NMe_2)_2]$ (5) (0.11 g, 0.35 mmol), $[Pt(PEt_3)_3]$ (0.19 g, 0.35 mmol), and benzene (10 mL) and heated to 85 °C for a period of 2 d. All volatiles were removed in vacuo, and the reddish-black residue was extracted with heptane (10 mL). After filtration through a pad of celite, the filtrate was reduced to 5 mL in volume and stored at −30 °C. $[V(\eta^6\text{-}C_6H_5BNMe_2)Pt(PEt_3)_2(\eta^6\text{-}C_6H_5BNMe_2)]$ (9) (0.23 g, 0.30 mmol, 87%) was isolated as black crystals that were subsequently washed with cold pentane (3 × 2 mL, −100 °C) and dried in vacuo. EPR (toluene, 140 K): ⟨g⟩ = 1.985; ⟨a⟩ (^{51}V) = 60.7 G. λ_{max} (ε) = 458 nm (2219 L mol^{-1} cm^{-1}). Anal. Calcd (%) for C$_{28}$H$_{52}$B$_2$N$_2$P$_2$PtV (746.31): C, 45.06; H, 7.02; N, 3.75. Found: C, 45.35; H, 6.65; N, 3.61.

$[V(\eta^6\text{-}C_6H_5BNMe_2)C(Me)=C(Me)(\eta^6\text{-}C_6H_5BNMe_2)]$, 10. (A) Stoichiometric Reaction. A solution of $[V(\eta^6\text{-}C_6H_5BNMe_2)Pt(PEt_3)_2(\eta^6\text{-}C_6H_5BNMe_2)]$ (9) (0.12 g, 0.16 mmol) in benzene (10 mL) in a resealable Schlenk flask equipped with a Teflon valve was treated with 2-butyne (322 μL, 1.60 mmol) and heated to 75 °C. After being stirred for 20 h, all volatiles were removed in vacuo and the black residue was subsequently extracted with hexanes (2 × 2 mL). Removal of all insolubles by filtration and storage at −60 °C afforded $[V(\eta^6\text{-}C_6H_5BNMe_2)C(Me)=C(Me)(\eta^6\text{-}C_6H_5BNMe_2)]$ (10) (0.04 g, 0.10 mmol, 63%) as a black, crystalline solid, which was washed with cold pentane (2 × 2 mL, −100 °C) and dried in vacuo.

(B) Homogeneous Catalytic Reaction. A solution of $[V(\eta^6\text{-}C_6H_5)_2B_2(NMe_2)_2]$ (5) (30.0 mg, 95.27 μmol) and $[Pt(PEt_3)_3]$ (2.6 mg, 7.76 μmol) in benzene (0.5 mL) was treated with 2-butyne (191 μL, 0.95 mmol) in a resealable J. Young NMR tube and heated to 95 °C over a period of 5 d. Subsequently, all volatiles were removed in vacuo, and the black residue was extracted with hexanes (5 mL). After filtration, the filtrate was reduced to 1.5 mL in volume and stored at −60 °C to yield the ansa-bis(boryl)alkene 10 (31.6 mg, 85.74 μmol, 90%) as a black crystalline solid after being washed with cold pentane (2 × 2 mL, −100 °C).

(C) Heterogeneous Catalytic Reaction. A solution of $[V(\eta^6\text{-}C_6H_5)_2B_2(NMe_2)_2]$ (5) (25.0 mg, 79.39 μmol) and Pd/C (5.1 mg, 4.76 μmol) in benzene (0.5 mL) was treated with 2-butyne (159 μL, 0.79 mmol) in a resealable J. Young NMR tube and heated to 95 °C over a period of 14 d. After removal of all volatiles in vacuo, the black residue was extracted with hexanes (3 mL) and filtrated into another flask by a filter canula. The black filtrate was reduced to 1 mL in volume and stored at −60 °C. The ansa-bis(boryl)alkene 10 (27.2 mg, 73.83 μmol, 93%) was isolated as a black crystalline solid after being washed with cold pentane (1 × 2 mL, −100 °C). EPR (toluene, 110 K): ⟨g⟩ = 1.986; ⟨a⟩ (^{51}V) = 61.7 G. MS (EI): m/z (%) = 369 (100) [M$^+$], 274 (13) [M$^+$ − V − NMe$_2$], 220 (12)

(43) Lauher, J. W.; Hoffmann, R. *J. Am. Chem. Soc.* **1976**, *98*, 1729.
(44) Fischer, E. O.; Reckziegel, A. *Chem. Ber.* **1961**, *94*, 2204.
(45) Haubold, W.; Kraatz, U. *Z. Anorg. Allg. Chem.* **1976**, *421*, 105.
(46) Nöth, N.; Schick, H.; Meister, W. *J. Organomet. Chem.* **1964**, *1*, 401.
(47) Yoshida, T.; Matsuda, T.; Otsuka, S. *Inorg. Synth.* **1990**, *28*, 119.
(48) Neese, F. *J. Chem. Phys.* **2003**, *118*, 3939.

$[M^+ - V - NMe_2 - C_2Me_2]$, 132 (18) $[PhBNMe_2^+]$, 91 (25) $[C_7H_7^+]$, 51 (18) $[M^+]$. λ_{max} (ε) = 455 nm (2130 L mol^{-1} cm^{-1}). Anal. Calcd (%) for $C_{20}H_{28}B_2N_2V$ (369.01): C, 65.07; H, 7.65; N, 7.59. Found: C, 64.99; H, 7.51; N, 7.33.

Crystal Structure Determinations. The crystal data of **3−6**, **9**, and **10** were collected at a Bruker X8Apex diffractometer with a CCD area detector and multilayer mirror monochromated Mo Kα radiation. The structure was solved using direct methods, refined with the SHELXL software package Sheldrick, G. M. SHELXL; : Göttingen, Germany, 1997 and expanded using Fourier techniques. All non-hydrogen atoms were refined anisotropically. Hydrogen atoms were assigned to idealized positions and were included in structure factor calculations.

Crystal data for **3·thf**: $C_{52}H_{76}Li_4O_7V_2$, M_r = 942.77, red block, $0.23 \times 0.18 \times 0.12$ mm^3, triclinic space group $P\bar{1}$, a = 10.1225(7) Å, b = 12.4870(8) Å, c = 19.2872(12) Å, α = 93.159(4)°, β = 90.694(4)°, γ = 93.629(4)°, V = 2429.0(3) Å^3, Z = 2, ρ_{calcd} = 1.289 g cm^{-3}, μ = 0.435 mm^{-1}, $F(000)$ = 1004, T = 100(2) K, R_1 = 0.0688, wR^2 = 0.1456, 14700 independent reflections [$2\theta \leq$ 61.44°], and 854 parameters. Because of high disorder of the thf solvent molecules, the bond distances were fixed within these groups during the refinement.

Crystal data for **4**: $C_{18}H_{24}BNV$, M_r = 316.13, brown needle, 0.23 $\times$ 0.09 $\times$ 0.045 mm^3, monoclinic space group $P2_1/n$, a = 6.2221(2) Å, b = 38.3377(11) Å, c = 13.3179(4) Å, β = 90.4200(10)°, V = 3176.78(17) Å^3, Z = 8, ρ_{calcd} = 1.322 g cm^{-3}, μ = 0.617 cm^{-2}, $F(000)$ = 1336, T = 100(2) K, R_1 = 0.0402, wR^2 = 0.0886, 6504 independent reflections [$2\theta \leq$ 52.8°], and 387 parameters.

Crystal data for **5**: $C_{16}H_{22}B_2N_2V$, M_r = 314.92, red block, 0.19 $\times$ 0.17 $\times$ 0.16 mm^3, monoclinic space group $P2_1/c$, a = 17.6200(3) Å, b = 8.8212(2) Å, c = 9.8947(2) Å, β = 91.3710(10)°, V = 1537.49(5) Å^3, Z = 4, ρ_{calcd} = 1.360 g cm^{-3}, μ = 0.637 mm^{-1}, $F(000)$ = 660, T = 100(2) K, R_1 = 0.0370, wR^2 = 0.0958, 4904 independent reflections [$2\theta \leq$ 62.98°], and 190 parameters.

Crystal data for **6**: $C_{16}H_{22}Si_2V$, M_r = 321.46, red block, 0.23 $\times$ 0.17 $\times$ 0.12 mm^3, orthorhombic space group $Pnma$, a = 13.2337(4) Å, b = 11.8332(3) Å, c = 9.8015(3) Å, V = 1534.89(8) Å^3, Z = 4, ρ_{calcd} = 1.391 g cm^{-3}, μ = 0.786 mm^{-1}, $F(000)$ = 676, T = 100(2) K, R_1 = 0.0282, wR^2 = 0.0748, 1586 independent reflections [$2\theta \leq$ 52.02°], and 97 parameters.

Crystal data for **9**: $C_{28}H_{50}B_2N_2P_2PtV$, M_r = 744.29, red block, 0.26 $\times$ 0.20 $\times$ 0.04 mm^3, orthorhombic space group $P2_12_12_1$, a = 11.5345(7) Å, b = 15.7328(10) Å, c = 17.2495(12) Å, V = 3130.3(4) Å^3, Z = 4, ρ_{calcd} = 1.579 g cm^{-3}, μ = 4.885 mm^{-1}, $F(000)$ = 1492, T = 293(2) K, R_1 = 0.0311, wR^2 = 0.0619, 6467 independent reflections [$2\theta \leq$ 53.24°], and 332 parameters.

Crystal data for **10**: $C_{20}H_{28}B_2N_2V$, M_r = 369.00, red block, 0.22 $\times$ 0.16 $\times$ 0.14 mm^3, monoclinic space group $P2_1/c$, a = 9.6364(7) Å, b = 11.5492(8) Å, c = 16.9744(12) Å, β = 90.00°, V = 1889.1(2) Å^3, Z = 4, ρ_{calcd} = 1.297 g cm^{-3}, μ = 0.529 mm^{-1}, $F(000)$ = 780, T = 100(2) K, R_1 = 0.0335, wR^2 = 0.0886, 3703 independent reflections [$2\theta \leq$ 52.1°], and 229 parameters.

Crystallographic data were also deposited with the Cambridge Crystallographic Data Centre. Copies of the data [**3−6**, **9**, **10**: CCDC 681364−681369] can be obtained free of charge via http://www.ccdc.cam.ac.uk/cgi-bin/catreq.cgi, by e-mailing data_request@ccdc.cam.ac.uk, or by contacting the Cambridge Crystallographic Data Centre, 12, Union Road, Cambridge CB 1EZ, UK; fax +44 1223 336033.

Theoretical Formalism and Computational Details. (A) Hyperfine Tensor Calculations. In the usual nonrelativistic first-order approximation, isotropic hyperfine splittings $a_{iso}(N)$ correspond to the Fermi contact term A_{FC}:

$$a_{iso}(N) = A_{FC} = \frac{4\pi}{3}\beta_e\beta_N g_e g_N \langle S_Z\rangle^{-1}\sum_{\mu,\nu} P_{\mu,\nu}^{\alpha-\beta}\langle\varphi_\mu|\delta(R_N)|\varphi_\nu\rangle \tag{1}$$

Here β_e is the Bohr magneton, β_N the nuclear magneton, g_N is the g-value of nucleus N, $\langle S_Z\rangle$ is the expectation value of the

z-component of the total electronic spin, and $P_{\mu,\nu}^{\alpha-\beta}$ is the spin-density matrix, and the summation runs over all occupied molecular orbitals. The components $T_{ii}(N)$ of the anisotropic tensor are given by

$$T_{ii}(N) = \frac{1}{2}\beta_e\beta_N g_e g_N \langle S_Z\rangle^{-1}\sum_{\mu,\nu} P_{\mu,\nu}^{\alpha-\beta}\left\langle\varphi_\mu\left|r_N^{-5}(r_N^2\delta_{ij} - 3r_{N,i}r_{N,j})\right|\varphi_\nu\right\rangle \tag{2}$$

where $r_N = r - R_N$ (R_N is the position vector of nucleus N). In the rest of this section, we will refer to the metal hyperfine interaction and omit subscript N. The second-order perturbation treatment of ref 42 is used to compute spin−orbit (SO) corrections to the hyperfine tensor. At the coupled-perturbed Kohn−Sham level, the dominant SO correction term arises as a second-order cross term between the one- and two-electron SO Hamiltonian H^{SO} and the perturbed Fock operator F'

$$A_{K,uv}^{SO-I} = \frac{1}{2}\alpha^4 g_e\gamma_K\frac{1}{2\langle S_Z\rangle} \times \left[\sum_k^{occ(\alpha)}\sum_a^{virt(\alpha)}\frac{\langle\psi_k^\alpha|h_u^{SO}|\psi_a^\alpha\rangle\langle\psi_a^\alpha|F'_v|\psi_k^\alpha\rangle}{\varepsilon_k^\alpha - \varepsilon_a^\alpha} - \sum_k^{occ(\beta)}\sum_a^{virt(\beta)}\frac{\langle\psi_k^\beta|h_u^{SO}|\psi_a^\beta\rangle\langle\psi_a^\beta|F'_v|\psi_k^\beta\rangle}{\varepsilon_k^\beta - \varepsilon_a^\beta}\right] \tag{3}$$

where α is the fine-structure constant, γ_K is the gyromagnetic ratio of the nucleus, h_{SO} is the one- and two-electron spin−orbit operator, F' is the perturbed Fock operator, with $F_v' = (l_v/r^3) - (2/\alpha)a_0\Sigma_{k=}^{\eta'^2}K_v'$, where (l_v/r^3) is the paramagnetic nuclear-spin electron-orbit operator, K_v' is a component of the response exchange operator, and a_0 is the weight of HF exchange depending on the specific hybrid functional used (see ref 48 for a related simultaneous CPKS implementation and also ref 42 for references to earlier work). ψ^σ and ε^σ are spin-polarized Kohn−Sham orbitals and orbital energies, respectively. GGA or LDA functionals led to an uncoupled DFT treatment for this second-order term (a_0 = 0).

(B) Computational Details. Initial coordinates were taken from the corresponding crystal structure analyses. The optimization was carried out with Gaussian03[49] at B3LYP[50] DFT level with 6-31G(d,p) basis set[51] for the nonmetal atoms and relativistic small core pseudopotentials[52] and corresponding valence basis sets for the metal atoms. Unrestricted Kohn−Sham wave functions were used.

Unrestricted Kohn−Sham single-point calculations were subsequently performed with Turbomole 5.9[53] using a 9s7p4d basis set for vanadium (specifically designed for hyperfine calculations)[38,50a,54] and flexible IGLO-II[55] basis sets for the ligand atoms. The following DFT exchange-correlation functionals were compared: the GGA functionals (a) BP86,[56] the hybrid functionals (b) B3LYP[50] with 20% exact exchange, (c) BHLYP[50a,57] with 50% exact exchange, as well as the user-defined hybrid functionals (d) B-30LYP with 30% exact exchange (70% E_X^{Slater} and 70% ΔE_x^{B88} and E_c^{LYP}), (e) B-35LYP with 35% exact exchange (65% E_X^{Slater} and 65%

(49) Frisch, M. J.; et al. *Gaussian 03*, revision C.02; Gaussian, Inc.: Wallingford, CT, 2004.

(50) (a) Becke, A. D. *J. Chem. Phys.* **1993**, *98*, 5648. (b) Stephens, P. J.; Devlin, F. J.; Chabalowski, C. F.; Frisch, M. J. *J. Phys. Chem.* **1994**, *98*, 11623.

(51) (a) Hehre, W. J.; Ditchfield, R.; Pople, J. A. *J. Chem. Phys.* **1972**, *56*, 2257. (b) Hehre, W. J.; Pople, J. A. *J. Chem. Phys.* **1972**, *56*, 4233.

(52) Dolg, M.; Wedig, U.; Stoll, H.; Preuss, H. *J. Chem. Phys.* **1987**, *86*, 866.

(53) Ahlrichs, R.; Bär, M.; Häser, M.; Horn, H.; Kölmel, C. *Chem. Phys. Lett.* **1989**, *162*, 165.

(54) Schäfer, A.; Horn, H.; Ahlrichs, R. *J. Chem. Phys.* **1992**, *97*, 2571.

(55) (a) Huzinaga, S. Ph.D. Thesis, University of Alberta, Edmonton, 1971. (b) Kutzelnigg, W.; Fleischer, U.; Schindler, M. *Deuterium and Shift Calculation*; NMR Basic Principles and Progress, Vol. 23; Springer: Berlin, 1990.

(56) (a) Becke, A. D. *Phys. Rev. A* **1988**, *38*, 3098. (b) Perdew, J. P. *Phys. Rev. B* **1986**, *33*, 8822.

(57) Lee, C.; Yang, W.; Parr, R. G. *Phys. Rev. B* **1988**, *37*, 785.

ΔE_x^{B88} and E_c^{LYP}), and (f) B-40LYP with 40% exact exchange (60% E_X^{Slater} and 60% ΔE_x^{B88} and E_c^{LYP}).

The unrestricted Kohn−Sham orbitals were transferred to the MAG-Respect property package[58] by suitable interface routines. The atomic mean-field approximation[59] was used to compute the matrix elements of the SO operator h_{SO} in eq 3.

Complex **9**, which was part of the experimental study, was not analyzed more closely here. It exhibited appreciable spin contami-

nation ($\langle S^2 \rangle = 1.791$ at B3LYP instead of the expected 0.75), and results were thus considered unreliable.

Supporting Information Available: Crystallographic data in CIF format. Graphical representations of the EPR spectra of compound **2**. Full list of authors for ref 49. Extended version of Table 5. Illustration of the spin-density distribution for complexes **1**, **2**, **4**−**7**, and **10**. This material is available free of charge via the Internet at http://pubs.acs.org.

JA802034P

(58) Malkin, V. G.; Malkina, O. L.; Reviakine, R.; Arbouznikov, A. V.; Kaupp, M.; Schimmelpfennig, B.; Malkin, I.; Helgaker, T.; Ruud, K. *MAG-Respect*, version 1.2; Julius-Maximilians-Universität Würzburg: Würzburg, Germany, 2003.

(59) (a) Hess, B. A.; Marian, C. M.; Wahlgren, U.; Gropen, O. *Chem. Phys. Lett.* **1996**, *251*, 365. (b) Schimmelpfennig, B. Ph.D. Thesis, Stockholms Universitet, Sweden, 1996.